EC3 design of web-post buckling resistance for perforated steel beams with elliptically-based web openings

Felipe Piana Vendramell Ferreira[a]*, Rabee Shamass[b], Luis Fernando Pinho Santos[b], Vireen Limbachiya[b], Konstantinos Daniel Tsavdaridis[c]

[a]Federal University of Uberlândia, Faculty of Civil Engineering – Campus Santa Mônica, Uberlândia, Minas Gerais, Brazil

[b]London South Bank University, School of Built Environment and Architecture, London, UK

[c]Department of Civil Engineering, School of Mathematics, Computer Science and Engineering, City, University of London, Northampton Square, EC1V 0HB, London UK

*Corresponding author

Abstract

In this paper, the influence of the web-post geometric parameters on the shear buckling resistance of perforated steel beams with previously proposed novel non-standard elliptically-based web openings is investigated. An economical and practical approach to estimate the web-post buckling resistance in accordance with EUROCODE 3 and the buckling resistance of the strut model analogy is developed and analysed. Finite element models are developed and validated against test results available in the literature. An extensive parametric study using Python code is carried out. A total of 5,400 geometrical models is investigated and the analysed parameters are discussed in relation to the buckling curves. It is concluded that the proposed design method for the web-post buckling resistance provides accurate and reliable predictions and can be used for practical design purposes of perforated steel beams with elliptically-based web openings.

Keywords: Steel beams; Elliptical web openings; Web-post buckling; Strut model; Eurocode 3.

E-mail adresses:

fpvferreira@ufu.br (F. P. V. Ferreira)

shamassr@lsbu.ac.uk (R. Shamass)

pinhosl3@lsbu.ac.uk (L. F. P. Santos)

limbachv@lsbu.ac.uk (V. Limbachiya)

konstantinos.tsavdaridis@city.ac.uk (K. D. Tsavdaridis)

Notation

The following symbols are used in this paper:

b_f	the flange width;	K	Coefficient in Eq. (19);
d	the parent section height;	l_{eff}	the web-post effective length;
d_g	the total height after castellation process;	R	the opening radius;
d_o	the opening height;	s	the web-post width;
d_t	the tee height;	t_f	the flange thickness;
$f_{cr,w}$	the critical shear stress in the web-post;	t_w	the web thickness;
f_y	the yield strength of the steel section;	V	the global shear;
f_u	the ultimate stress of the steel section;	w	the opening width;
h	the distance between flanges geometric centres of the parent section;	ε	strain;
		λ_0	the reduced slenderness factor;
H	the distance between flanges geometric centres after castellation process;	λ_w	the web-post slenderness factor;
		σ	stress;
k	Coefficient in Eq. (10);	χ	the reduction factor;

1. INTRODUCTION

Perforated steel beams with periodical web openings are manufactured using the castellation process (aka profile cutting procedure), which consists of three steps: thermal cutting of the initial (parent) section, separation of the two halves, and welding. The result of this process is an expanded (deeper) section. The steel beams with periodical web openings are classified based on the shape of the web opening. The castellated, cellular and Angelinas™ [1] beams are those with hexagonal, circular and sinusoidal web openings, respectively. These steel beams have been used in construction, mainly due to many advantages such as greater flexural stiffness due castellation process, self-weight reduction and structural floor height reduction as the web openings allow the integration of hydraulic and electric services (instead of them running under the steel beams).

The flexural behaviour of the perforated steel beams with periodical web openings can be a complex problem as they are prone to several failure modes such as a plasticisation mechanism, due to the Vierendeel bending, and buckling modes such as lateral-torsional, web-post[1], web distortional or even the combination between them [2–8]. The present study focuses on the web-post buckling failure which occurs for steel beams with closely spaced periodical web openings that have thin-walled nature [9]. It is a local phenomenon, in which the final configuration of the web-post is characterised by a lateral displacement with torsion due to the horizontal shear at the web-post. The main geometric parameters that influence the web-post buckling resistance are the opening height, the web-post width, and the web thickness [10–13]. In the literature, various research recommendations were suggested to predict the web-post buckling resistance of perforated steel beams. For example, Fares et al. [13] published recommendations and design guidance for cellular and castellated steel beam in accordance with ANSI/AISC 360-16 [14]. Their design guidance is based on an early empirical design method in Ward's work [15]. On the other hand, Lawson and Hicks [16] suggested different design method to calculate the web-post buckling resistance of cellular beams with and without elongated openings based on the design of compressed diagonal strut and the compressive stress is calculated according to EC3 [17], while the web-post buckling resistance of Angelinas™ can be obtained from the software ACB+ developed by Centre Technique Industriel de la Construction Métallique (CTICM) for ArcelorMittal [1].

---

[1]The Angelinas™, although they present a buckling mode in the web-post, this mode is not characterised as a double curvature in an "S" shape, such as the web-post buckling of castellated and cellular beams.

Researchers sought to optimise the opening shape for a better distribution of stresses, and consequently, the increase of resistance. In this context, the works of Tsavdaridis and D'Mello [20], Tsavdaridis [21] and Tsavdaridis et al. [22] are highlighted. Early works of Tsavdaridis and D'Mello [23] investigated the Vierendeel bending and web-post buckling resistance of steel beams with various non-standard web openings. It was highlighted that vertical elliptical (vertical major axis) web openings presented positive results. In particular, the optimised novel elliptically-based web openings provided smooth edges that resisted the formation of plastic hinges at low values of load while the stress concentration is controlled and occured at positions nearer to the neutral axis – at the intersection of the semi-circle and the lines [10,23,24]. Perforated beams with non-standard web openings were patented (GB 2492176 [25]) by the authors.

Specifically, in Tsavdaridis and D'Mello [10] tests were carried out on short span steel beams with different web openings shapes (i.e. circular with and without fillets and elliptically-based), considering three-point bending. In this study, the web-post resistance was main failure to be investigated. Finite element models were validated and parametric studies were conducted varying the ratios of web-post width to opening height and opening height to web-thickness. The authors concluded that elliptically-based web openings had shown better stress distribution and greater resistance to horizontal shear stresses in comparisons with circular web openings. Also, the authors proposed an equation to predict the web-post buckling resistance by global shear based on parameters studied. Importantly, this equation is applied to d_o/t_w=30-80.77 and t_w=3.9-10.5mm. Later, Tsavdaridis and D'Mello [24] conducted an optimisation study of these elliptically-based web openings and their resistance to the Vierendeel mechanism. In this work, which was based on the finite element method, the authors concluded that the elliptical web openings presented an increase in the flexural stiffness. Consequently, steel beams with elliptically-based web openings presented lower deflections when compared to steel beams with web circular openings.

Limited investigation has been carried out on perforated steel beams with elliptically-based web openings. For practical and design purposes, this paper aims to investigate the web-post buckling resistance of steel beams with elliptically-based web openings (**Fig. 1**), as it is the most critical failure mode for such kind of structural members. The procedure is based on defining the effective length of diagonal strut analogy in the web-post while the buckling resistance of the compressed struct is calculated using EC3 [17]. As seen in the **Fig. 1**, b_f, t_f, t_w and d are the flange width and thickness, web thickness and the height of the parent section, respectively, H is the cellular beam height after castellation process, d_o, w and R are the opening height, width and radius, respectively, and s and b_w are the opening spacing and web-post width, respectively. For this task, a finite element models were developed and validated against the tests data conducted by Tsavdaridis and D'Mello [10]. A parametric study is carried out, considering buckling, post-buckling and geometrical nonlinear analyses. The geometric parameters ratios d/H, d_o/H, R/d_o and w/d_o are varied with respect to the castellation process. A total of 5,400 geometrical models is analysed. The numerical results are used to developed an equation in line with EC3 [17]. In the next section, the development of the finite element model is presented.

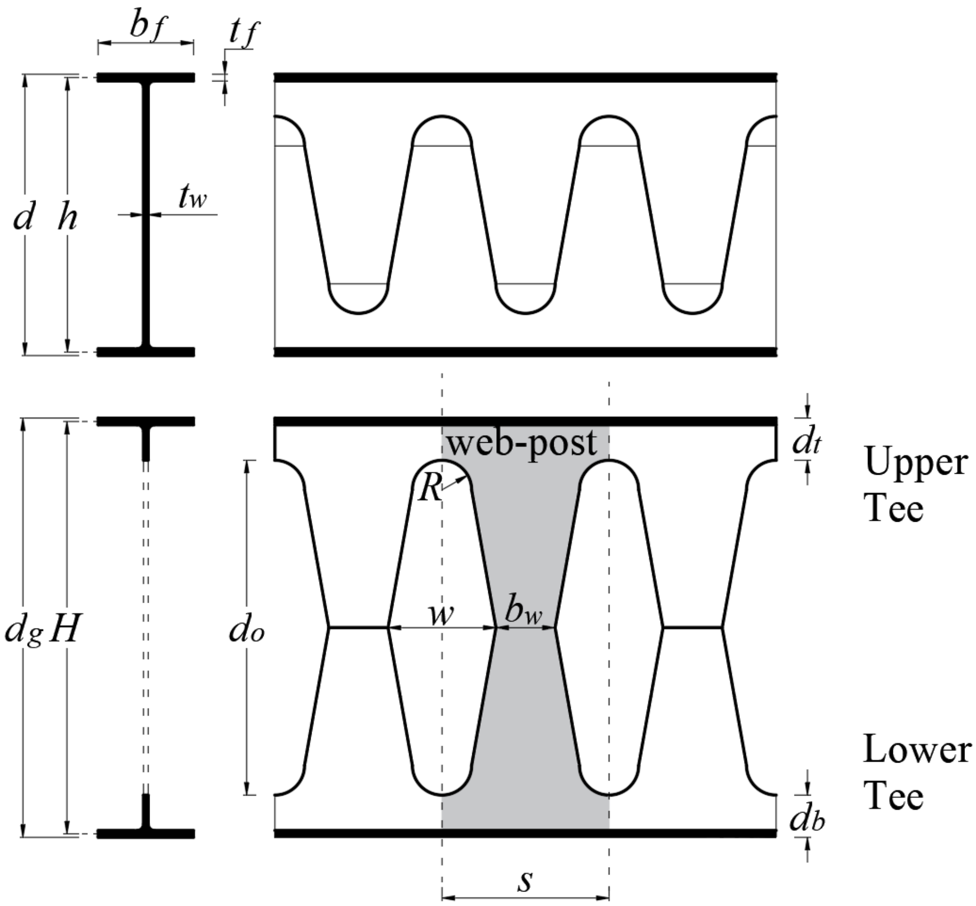

Fig. 1: Castellation process of steel beams with elliptically-based web openings [24]

2. FINITE ELEMENT ANALYSIS

The validation study is presented in two steps. Initially, the modelling is performed based on the experimental tests carried out in Tsavdaridis and D'Mello [11]. These models will be called here as full models. In the second part, single web-post models are developed. This approach has been widely used by researchers i.e. Zaarour and Redwood [25], Panedpojaman et al. [13], Tsavdaridis and Galiatsatos [26], Durif et al. [27], Grilo et al. [10], Limbachiya and Shamass [12], as it is possible to analyse separately the main parameters that influence the web-post buckling resistance, such as the web-post width and the opening height.

All models are processed in the ABAQUS software in two steps: buckling and post-buckling analyses. The geometrically and materially nonlinear analysis with imperfections included (GMNIA) has been used by researchers of steel beams with periodical web openings, i.e. Ferreira et al. [28–33], Komal et al. [34], Ellobody [3,5], Panedpojaman et al [4] and Shamass and Guarracino [35]. The imperfection factor adopted was d_g/500. This factor was also used by Panedpojaman et al. [13], since the estimation of physical and geometric imperfections on steel beams with web openings is complex due to the manufacturing processes. Nominal strength values of the S355 steel are used[2]. The modulus of elasticity and Poisson's coefficient are taken equal to 200GPa and 0.3, respectively. A multi-linear constitutive model (**Fig. 2**) is considered, similarly to the methodology applied in Shamass and Guarracino [35]. The values of ε_{sh} and ε_u were calculated as Yun and Gardner [36], according to the **Eqs. (1-2)**. The stress- strain relationship implementation must be done with the real values (**Eqs. 3-4**).

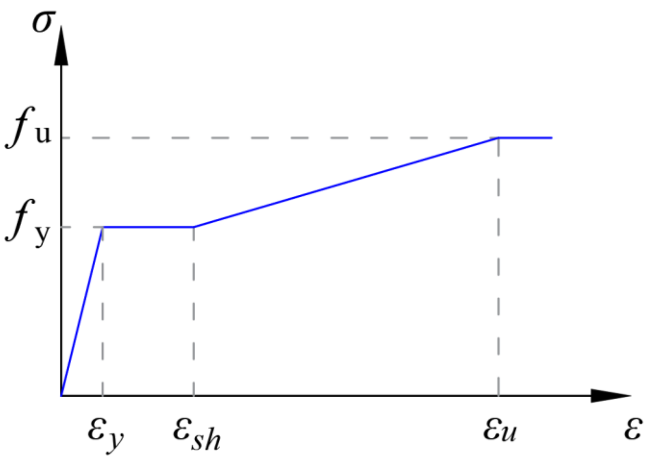

Fig. 2: Multi-linear constitutive model for steel

$$\varepsilon_u = 0.6\left(1 - \frac{f_y}{f_u}\right), \quad \varepsilon_u \geq 0.06 \tag{1}$$

$$\varepsilon_{sh} = 0.1\frac{f_y}{f_u} - 0.055, \quad 0.015 < \varepsilon_{sh} \leq 0.03 \tag{2}$$

[2]According to tensile coupon tests performed by Tsavdaridis and D'Mello [11], the yield strength of the web and flange/stiffener were 375.3MPa and 359.7MPa, respectively, and the ultimate stresses were 492.7MPa and 480.9MPa for web and flange/stiffener, respectively. These values are close to the nominal strength values of S355.

$$\sigma^{true} = \sigma^{nom}\left(1+\varepsilon^{nom}\right) \tag{3}$$

$$\varepsilon^{true} = \ln\left(1+\varepsilon^{nom}\right) \tag{4}$$

Based on the mesh sensitivity analysis and recommendation by Ferreira et al. [31] and Ferreira and Martins [7], the element mesh size taken was 10 mm. The steel beam and stiffnesses were modelled using a general-purpose three-dimensional reduced integration shell element, named S4R. S4R has six degrees of freedom - three rotations and three translations that provide accurate results with less computational effort. The boundary conditions used for the full and single web-post models, as well as the validation results, are presented in the subsections below.

2.1 FULL MODELS

The experimental tests employed for the validation study are conducted by Tsavdaridis and D'Mello [11]. Specimens A1 and B1 are cellular beams with circular web openings opening, and specimen A2 is a cellular beam with fillets introduced at the mid-depth of the cellular web opening to ease their fabrication. B2 and B3 are perforated sections with the proposed novel vertical elliptically-based web openings. The boundary conditions of the full models are shown in **Fig. 3**. The analysis is performed with load control and the arc-length method is employed to capture the buckling behaviour. At the bottom of the stiffener in one end, vertical and longitudinal displacements are restrained (Uy=Uz=0). At the bottom of the stiffener in the other end, only the vertical displacement is restrained (Uy=0). At both ends, in the region of the stiffeners, lateral displacement and the rotation around the longitudinal axis are restrained at four points (Ux=URz=0).

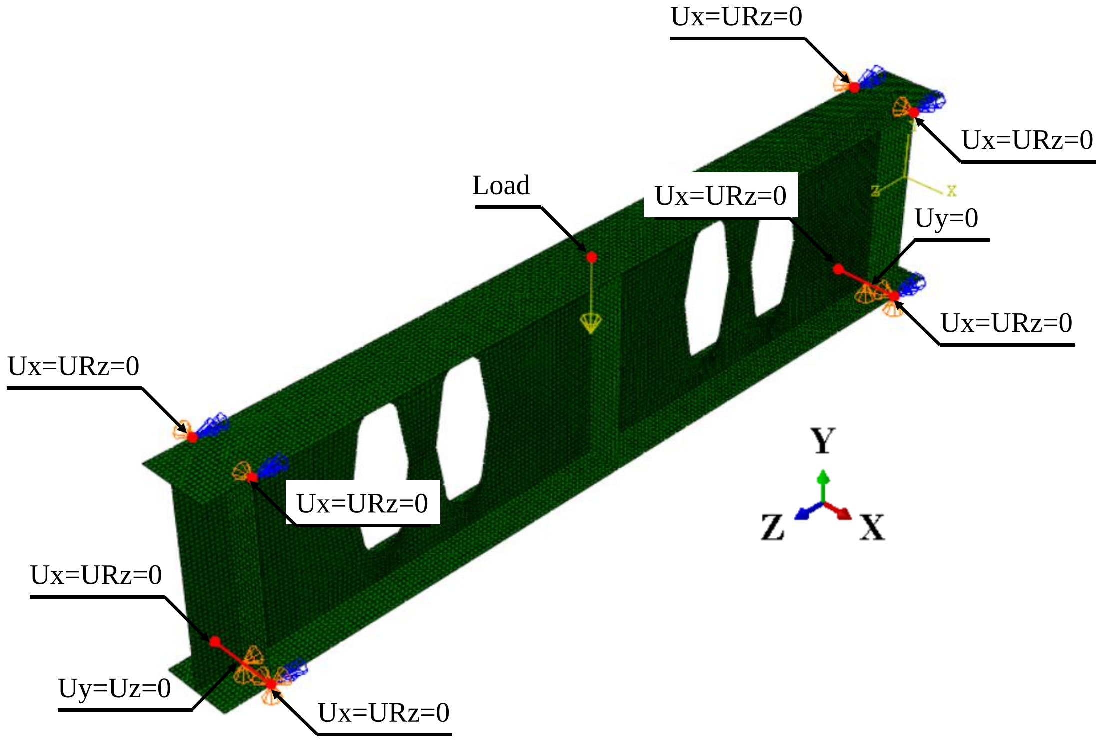

Fig. 3: Boundary conditions of the full models, considering B3 model

The validation results are presented by comparing the equilibrium trajectories of both tests and full models, considering the load-deflection relationships (**Fig. 4**). As shown in the models A1 (**Fig. 4a**), A2 (**Fig. 4b**), B1 (**Fig. 4c**), B2 (**Fig. 4d**) and B3 (**Fig. 4e**), the load-displacements relationships of numerical models are in agreement with tests. The deformed beams tested by Tsavdaridis and D'Mello [11], are compared with the results of the finite element method (**Fig. 5**). It is possible to notice that in all analyses, considering the models A1 (**Fig. 5a**), A2 (**Fig. 5b**), B1 (**Fig. 5c**), B2 (**Fig. 5d**) and B3 (**Fig. 5e**), the mode of failure was characterised by web-post buckling, similarly to the tests. Furthermore, in **Table 1**, the values of the peak load of the tests and numerical models are summarised. In view of the results presented so far, it is possible to conclude that the numerical models are adequately validated, since the results showed a low relative error in comparison to the tests.

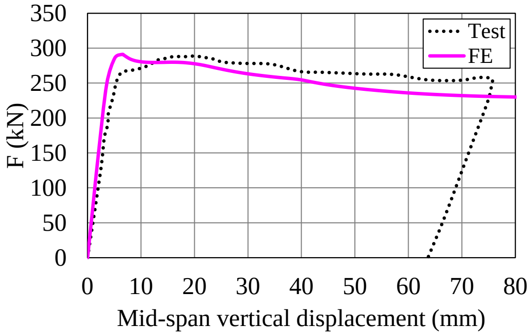

(a) A1

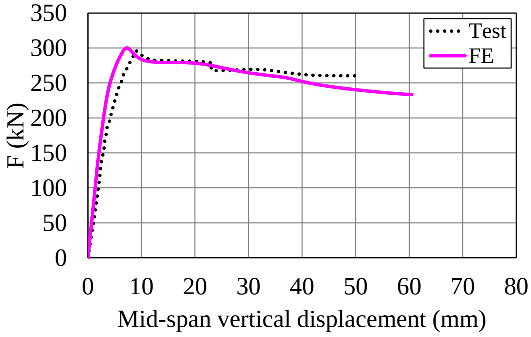

(b) A2

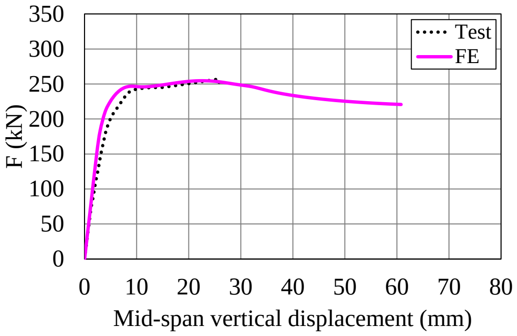

(c) B1

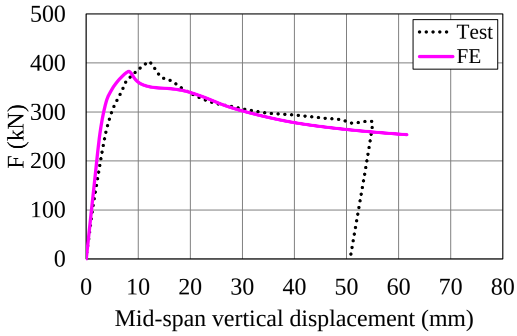

(d) B2

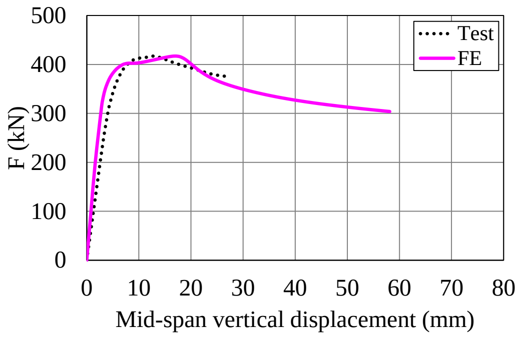

(e) B3

Fig. 4: Tests and finite element model by load-displacement relationships

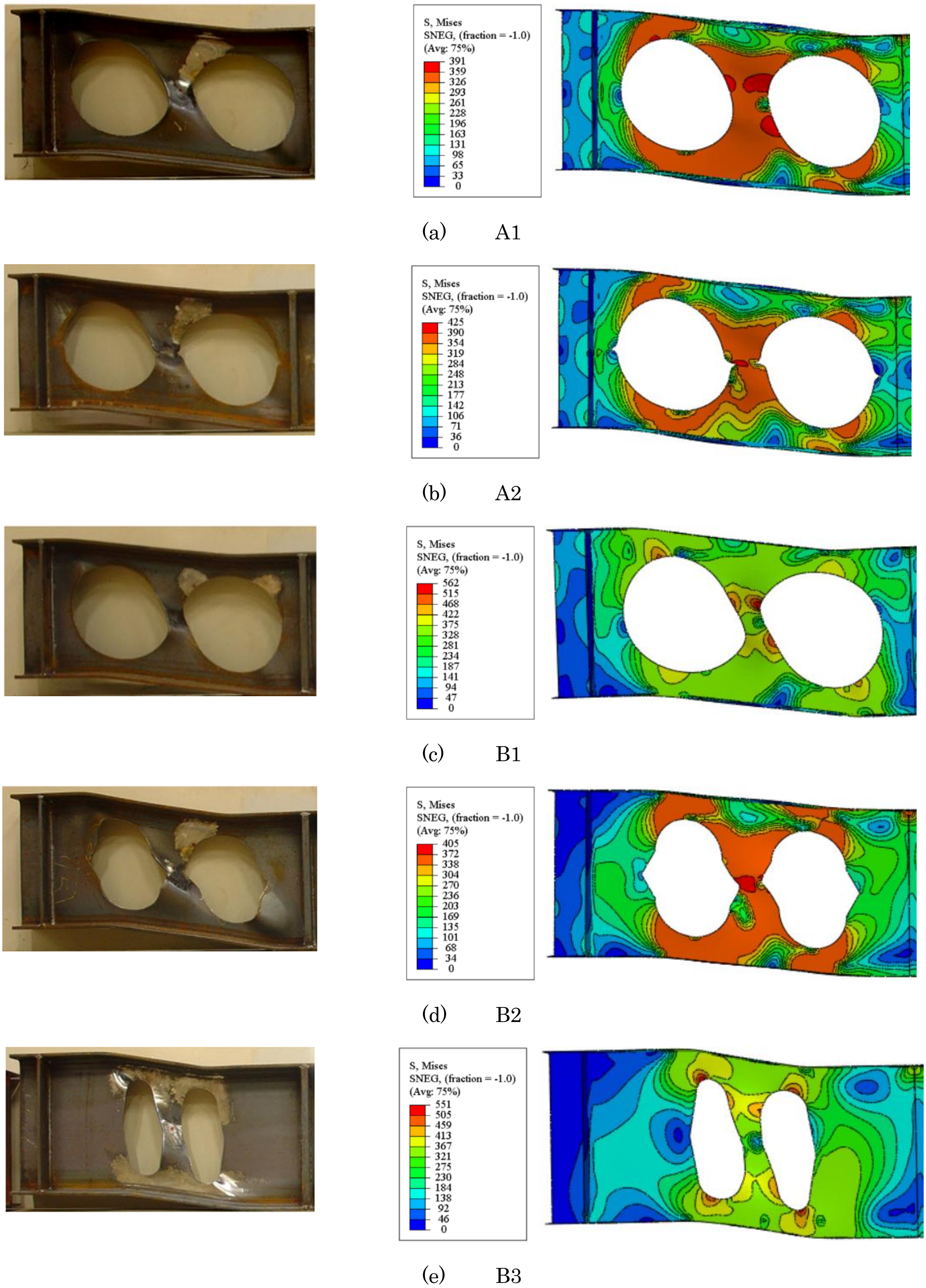

Fig. 5: Final configuration between tests performed by Tsavdaridis and D'Mello [11] with finite element model

Table 1: Summary of full models results

Test	F_{Test} (kN)	F_{FE} (kN)	$(F_{FE}/F_{Test}$-1)%	Failure
A1	288.7	291.0	0.8%	WPB
A2	298.0	300.0	0.7%	WPB
B1	255.0	254.5	-0.2%	WPB
B2	402.4	382.7	-4.9%	WPB
B3	415.0	417.1	0.5%	WPB

2.2 SINGLE WEB-POST MODELS

Single web-post models were also developed and validated to conduct parametric studies. After several trials and comparisons with the test results, the boundary conditions shown in in **Fig. 6** were used, leading to reasonably accurate predictions. On one end, at both the flange and web of the tee sections, lateral, vertical and longitudinal displacements are restrained (Ux=Uy=Uz=0). On the other end, lateral displacement as well as rotations about the vertical and longitudinal axes are restrained (Ux=URy=URz=0) at the flanges of both upper and lower tees. At that same end, lateral displacement as well as rotations about to the lateral and vertical axes are restrained at the webs of both upper and lower tees (Ux=URx=URy=0). Finally, the shell edge load was applied along the web of the tee sections on the right hand side of the model, as seen in the **Fig. 6.** The mesh size used in this model was of 3mm and 8mm for web and flanges, respectively. In **Table 2**, the shear load results calculated from FE (V_{FE}) are compared with those obtained from the tests (V_{Test}). It can be noted that the percentage difference between FE and the test shear loads varies between 9.4% to -8.8% with an average of -0.14% and coefficient of variation of 0.14%. Hence, the proposed web-post model can be reasonably accurate and used for further parametric studies to predict the shear load capacity of the web-post.

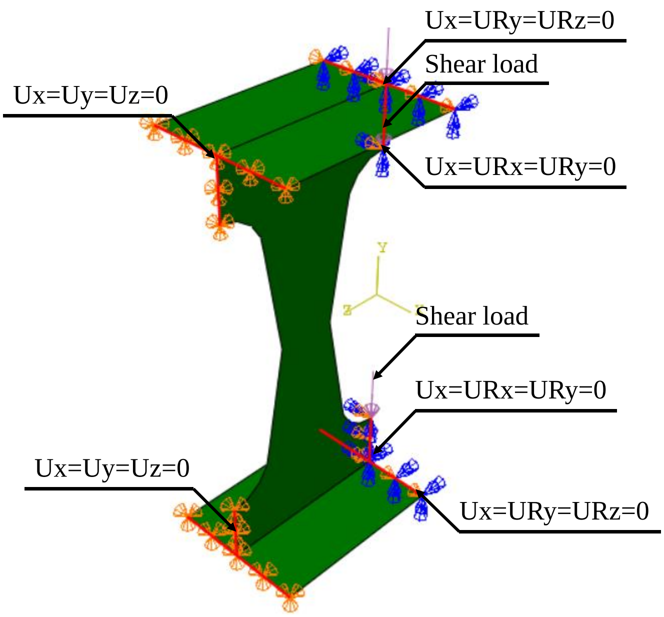

Fig. 6: Boundary conditions of the web-post models

Table 2: Summary of web-post models results

Test	V_{Test} (kN)	V_{FE} (kN)	Failure	$(V_{FE}/V_{Test}-1)\%$
A1	144.4	157.0	WPB	8.8%
A2	149.0	159.0	WPB	6.7%
B1	127.5	121.0	WPB	-5.1%
B2	201.2	200.5	WPB	-0.3%
B3	207.5	188.0	WPB	-9.4%
			S.D.	6.93%
			Var.	0.48%

2.3 PARAMETRIC STUDY

In total, twelve UB sections are considered (**Table 3**). For each UB section, the geometric ratios H/d, d_o/H, R/d_o and w/d_o are varied (**Fig. 1**) with respect to the castellation process (**Eq. 5**). The variations performed are:

- H/d=1.2, 1.3, 1.4, 1.5 and 1.6;
- d_o/H=0.65, 0.70, 0.75, 0.80, 0.85 and 0.90;
- R/d_o=0.10, 0.15, 0.20, 0.25, 0.30, 0.35 and 0.40;

- w/d_o=0.25, 0.35, 0.45, 0.55 and 0.65.

$$H = 2h - 2d_t - 2R \tag{5}$$

Table 3: UB sections

UB Section	d (mm)	b_f (mm)	t_f(mm)	t_w (mm)
178x102x19	177.8	101.2	7.9	4.8
305x102x25	305.1	101.6	7.0	5.8
305x102x33	312.7	102.4	10.8	6.6
305x127x48	311.0	125.3	14.0	9.0
457x152x52	449.8	152.4	10.9	7.6
457x191x133	480.6	196.7	26.3	15.3
533x210x122	544.5	211.9	21.3	12.7
533x312x272	577.1	320.2	37.6	21.1
686x254x170	692.9	255.8	23.7	14.5
838x292x176	834.9	291.7	18.8	14.0
914x305x201	903.0	303.3	20.2	15.1
1016x305x487	1036.3	308.5	54.1	30.0

Each model of the parametric study is processed in two steps, (1) eigenvalue buckling analysis followed by (2) geometrical nonlinear analyses with imperfections. In addition, geometrical nonlinear analysis without imperfections is considered. The geometric nonlinear analysis with imperfections is performed with the objective of defining the web-post buckling mode and obtain the capacity resistance of the structural component. Python script is developed to conduct the parametric study as well as post-process the results.

The script can create the FE model for a given web geometry defined by the parameters in **Fig 1** and the boundary condition shown in **Fig.6**. The script firstly performed eigenvalue buckling analysis to define the lowest buckling mode that was used as initial imperfection shape while the imperfection size was $d_g/500$. Then, it performed nonlinear analysis using a Newton-Raphson solution method in order to obtain the buckling load, while both the buckling load and the failure mode were stored for analysis. The script is publicly available at https://github.com/luisantos090/WPB.

3. RESULTS AND DISCUSSION

From the 5,400 geometrical models analysed, 4,344 models had the resistance defined by web-post buckling. The results are discussed, considering the influence of the parameters, as well the web-post buckling resistance according to EC3 buckling curves [18], which are presented in the **Eq. (6-8)** and **Table 4**.

$$\chi = \frac{1}{\phi + \sqrt{\phi^2 - \lambda_0^{\,2}}} \leq 1.0 \tag{6}$$

$$\phi = 0.5\left[1 + 0.49\left(\lambda_0 - 0.2\right) + \lambda_0^{\,2}\right] \tag{7}$$

$$\lambda_0 = \sqrt{\frac{f_y}{f_{cr,w}}} \tag{8}$$

Table 4: Imperfection factors for buckling curves

Buckling curve	*a*	*b*	*c*	*d*
Imperfection factor (α)	0.21	0.34	0.49	0.76

The results of elastic buckling (from the eigenvalue analysis), and post-buckling analyses (i.e., web-post buckling resistance) are normalised in accordance with the EC3 buckling curves, considering the parent section and H/d, d_o/H, R/d_o and w/d_o ratios. A similar analysis was presented in Ferreira et al. [28], however, it considered steel-concrete composite cellular beam models and focused on web-post buckling resistance. It is important to highlight that SCI P355 [17] employed the strut analogy for calculating the web-post buckling resistance. In this model, the buckling compressive stress of the strut with an effective length, is calculated according to EC3, in a similar way of calculating the plastic buckling of compression members. The choice of buckling curve is a function of the geometric parameters of the steel profile, such as the flange thickness and width and the cross section height. For cellular steel beams with periodical circular web openings, SCI P355 [17] recommends using the buckling curve b and the buckling curve c for hot-rolled and welded (plated) sections, respectively. It is important to note that due to the castellation process, steel beams with elliptically-based web openings undergo the welding process, according to **Fig.** 1, hence, buckling curve c was chosen.

To normalise the numerical results with the EC3 buckling curves, the critical ($f_{cr,w,FE}$) and ultimate ($\sigma_{u,FE}$) shear stresses acting in the web-post, which are predicted by the critical ($V_{cr,FE}$) and ultimate ($V_{u,FE}$) shear forces considering buckling and post-buckling analyses, respectively, and are calculated according to **Eqs. (9-10)**. The normalised results, which are obtained by using the nominal values of S355 steel, are shown in **Fig. 7**. The geometric parameters of the web-post of perforated steel beams with elliptically-based web openings were presented in **Fig. 1**.

$$f_{cr,w,FE} = \frac{V_{cr,FE}}{t_w\left(s-w\right)} \tag{9}$$

$$\sigma_{u,FE} = \frac{V_{u,FE}}{t_w\left(s-w\right)} \tag{10}$$

3.1 *H/d* ratio

The H/d ratio refers to the expansion factor, that is, the ratio of the height of the section with the elliptically-based web opening to the parent section, according to **Fig. 1**. **Fig. 7** shows the normalised results for the EC3 buckling curves, considering the expansion factor variation. Each series is presented in two figures. The first one shows the maximum values of resistance, and the second one is a zoom in of the first graph to better show the results and the buckling curves. The expansion factors were *H* / *d*=1.1 (**Fig. 7a**), *H* / *d*=1.2 (**Fig. 7b**), *H* /*d*=1.3 (**Fig. 7c**), *H* / *d*=1.4 (**Fig. 7d**), *H* / *d*= 1.5 (**Fig. 7e**), *H* /*d*= 1.6 (**Fig. 7f**), *H* / *d*= 1.7 (**Fig. 7g**), *H* /*d*= 1.8 (**Fig. 7h**) and *H* /*d*= 1.9 (**Fig. 7i**). It was verified that the smaller the expansion factor, the smaller the web-post slenderness, and consequently, the smaller the effective length. This causes an increase in capacity resistance. However, the greater the reduced slenderness (λ_0), the lower the capacity resistance. It is important to highlight that although the results shown here illustrate the response as a function of the expansion factor (*H*/*d*) with respect to the castellation process, there were models that vary the other geometric parameters of the section with these elliptically-based web openings for the same expansion factor, such as the opening height, the web-post width and the opening radius. Once these parameters were varied, the effective length changes, and consequently, the web-post buckling resistance changes. The effective length will be presented in section 4 with more details.

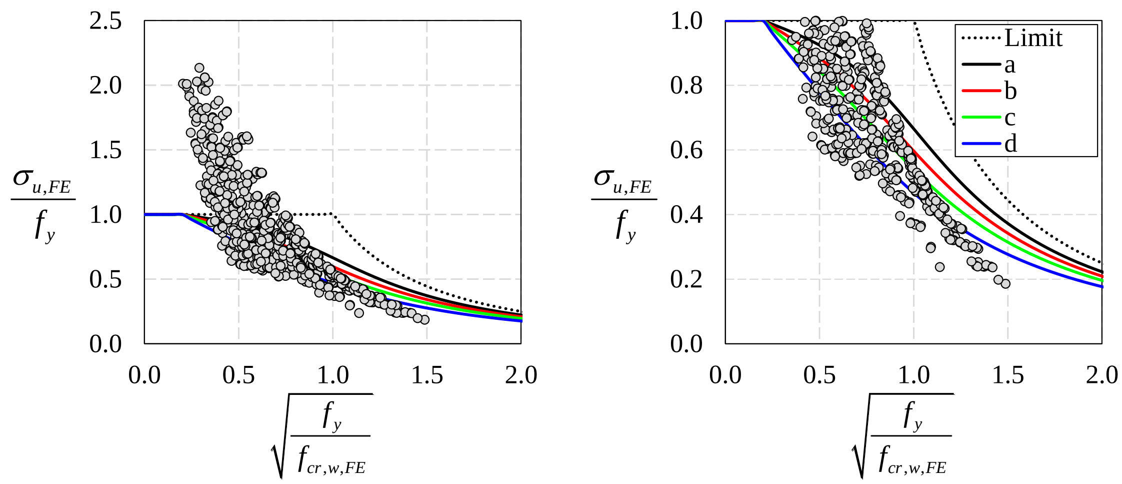

(a) *H*/*d*=1.2

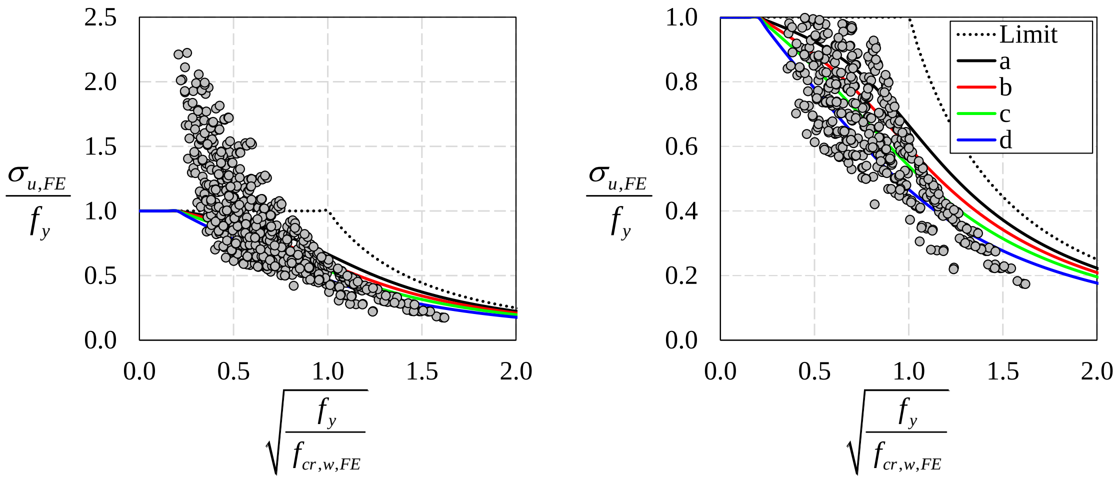

(b) *H/d=1.3*

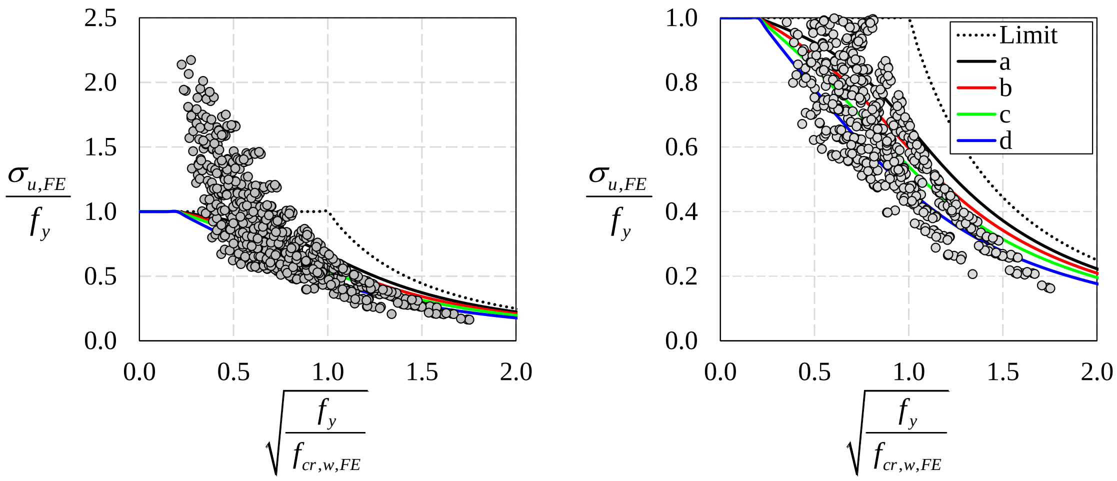

(c) *H*/*d*=1.4

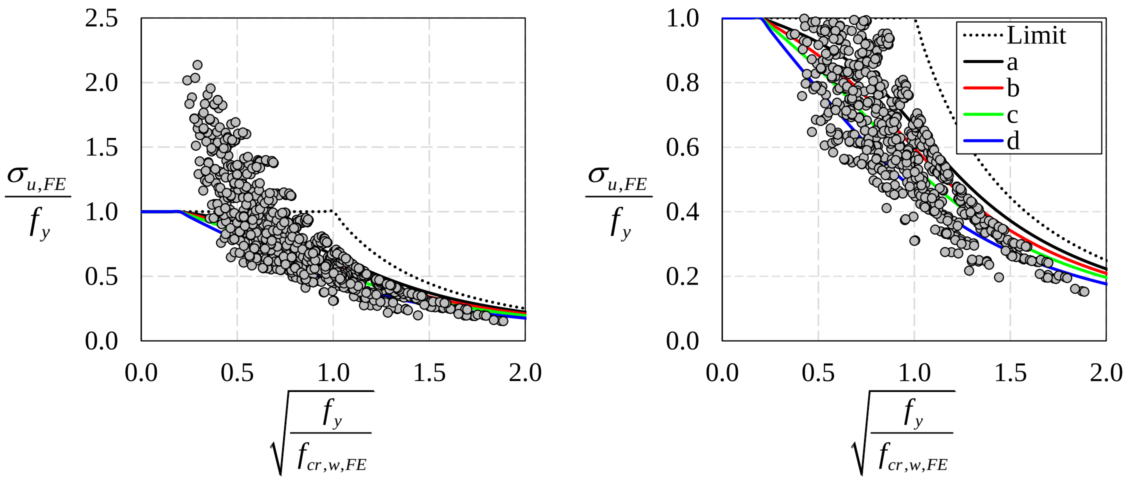

(d) *H*/*d*=1.5

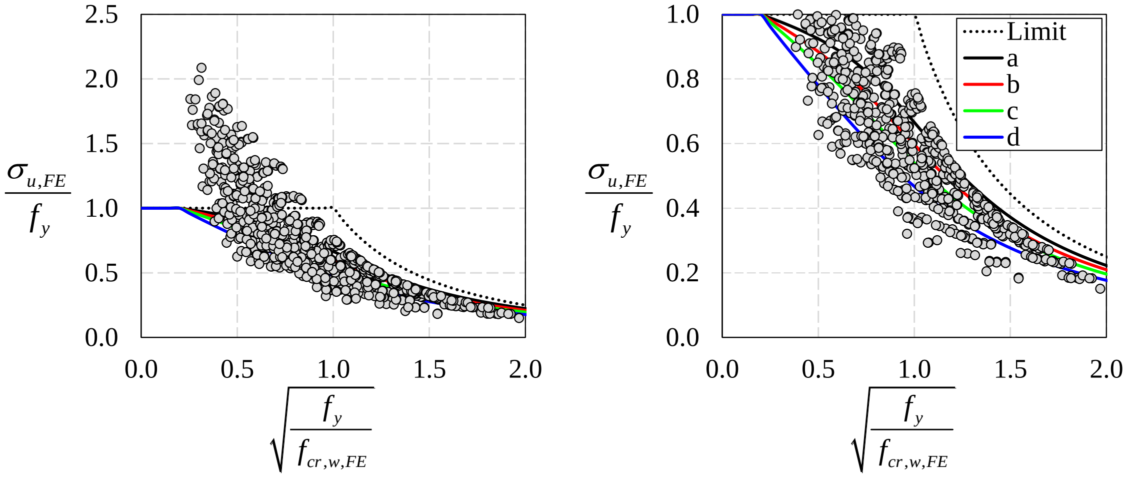

(e) H/d=1.6

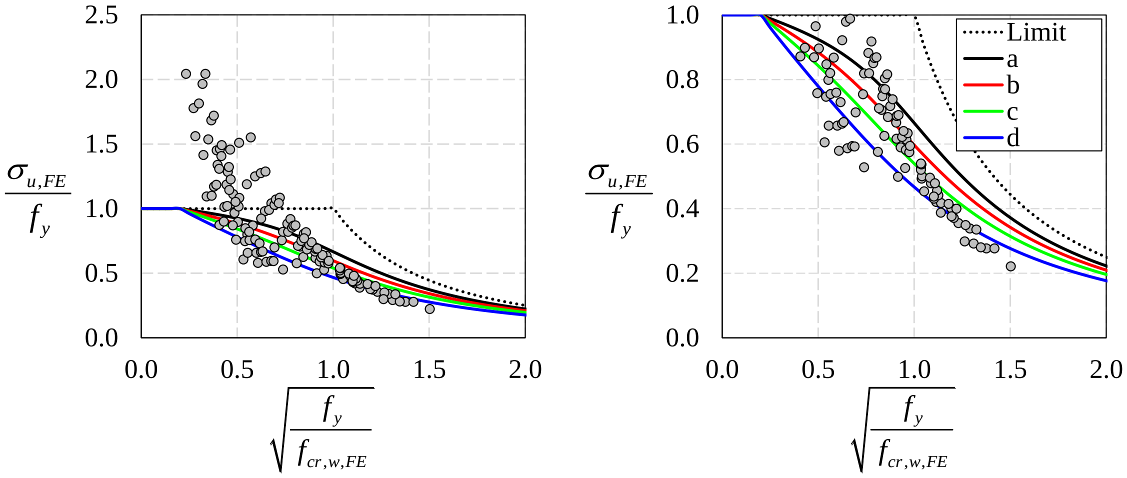

(f) H/d=1.7

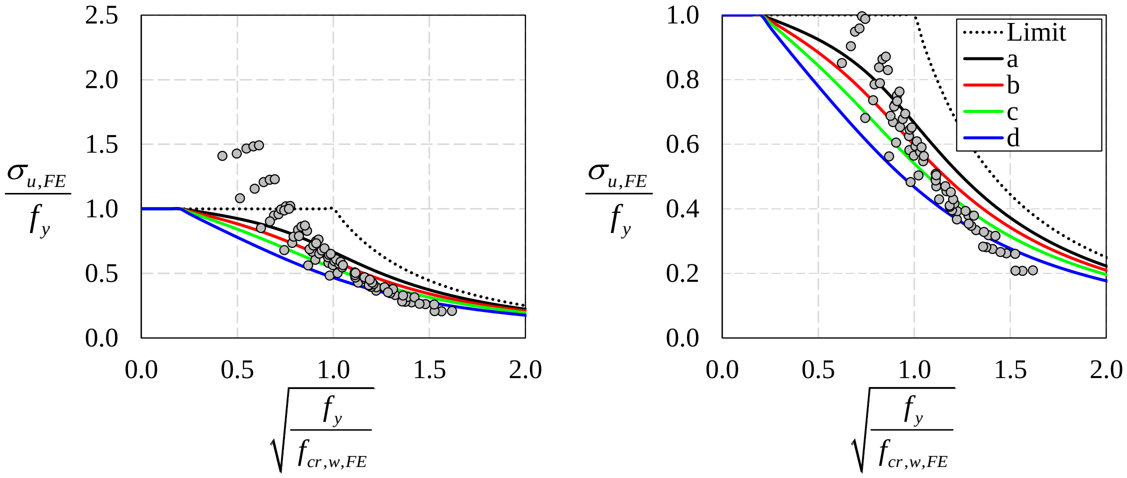

(g) H/d=1.8

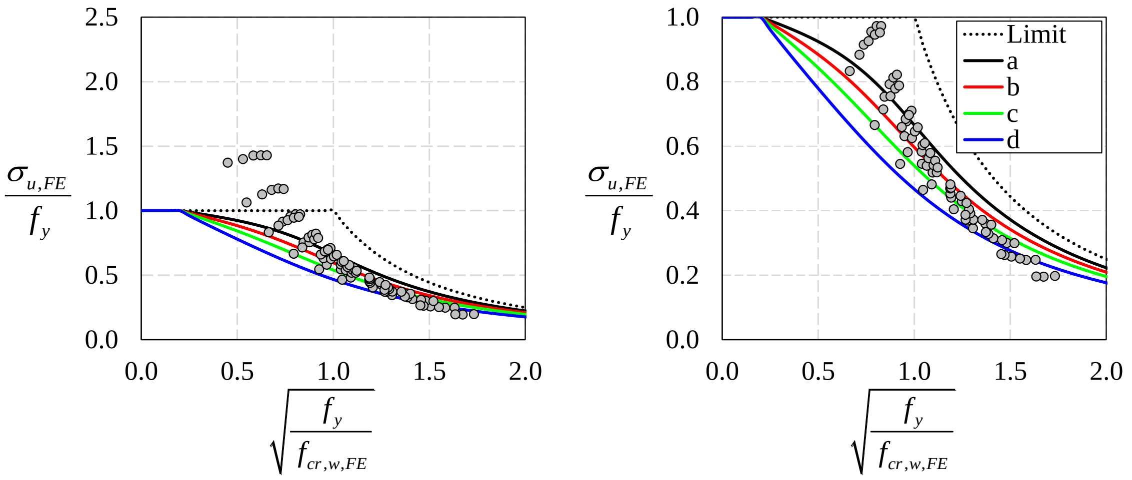

(h) H/d=1.9

Fig. 7: *H/d* ratio vs. buckling curves of EC3

3.2 d_o/H ratio

Fig. 8 shows the EC3 buckling curves in relation to the ratio of parameters that take into account the opening height variation to the final web height, after the castellation process. The results are illustrated considering d_o/H=0.65 (**Fig. 8a**), d_o/H=0.70 (**Fig. 8b**), d_o/H=0.75 (**Fig. 8c**), d_o/H=0.80 (**Fig. 8d**), d_o/H=0.85 (**Fig. 8e**) and d_o/H=0.90 (**Fig. 8f**). According to the results presented, it is possible to highlight that the lower the opening height, the greater the resistance. This can be explained in terms of the upper and lower tees sections, that is, the lower the height of the web opening is, the greater the height of the tee sections is, thus increasing the capacity to resist normal and tangential stresses.

Another point to be discussed refers to reduced slenderness (λ_0). For the range $0.65 \leq d_o/H \leq 0.80$ and considering $\lambda_0<1.0$, it was verified that the maximum values of resistance exceeded the limit of resistance ($\sigma_{u,FE}/f_y>1.0$), and the minimum values of resistance laid close to the buckling curve *d*. On the other hand, considering the ratio variation in $0.85<d_o/H \leq 0.90$, there was a drop in capacity resistance. For these analysed models, it was verified that the maximum resistance values lie above the buckling curve

a, however, lower than the limit value ($1/\lambda_0^2$). Regarding the range of the ratio in $0.85<d_0/H\leq0.90$, it was observed that some models indicated resistance below the buckling curve *d* for values $\lambda_0<1.0$. This can be explained by the fact that their tee sections experienced instability phenomena before reaching the yield strength, for small values of applied loading.

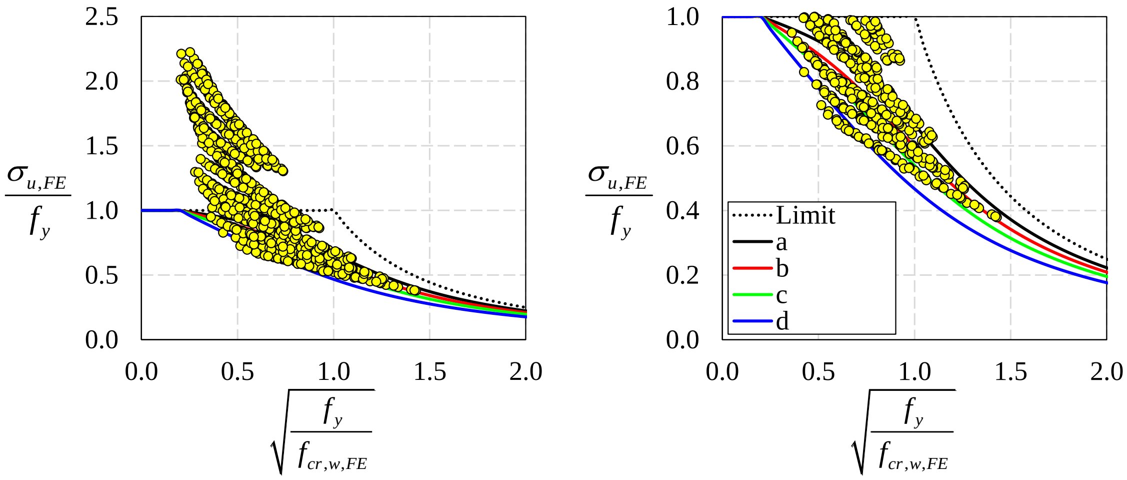

(a) d_0/H=0.65

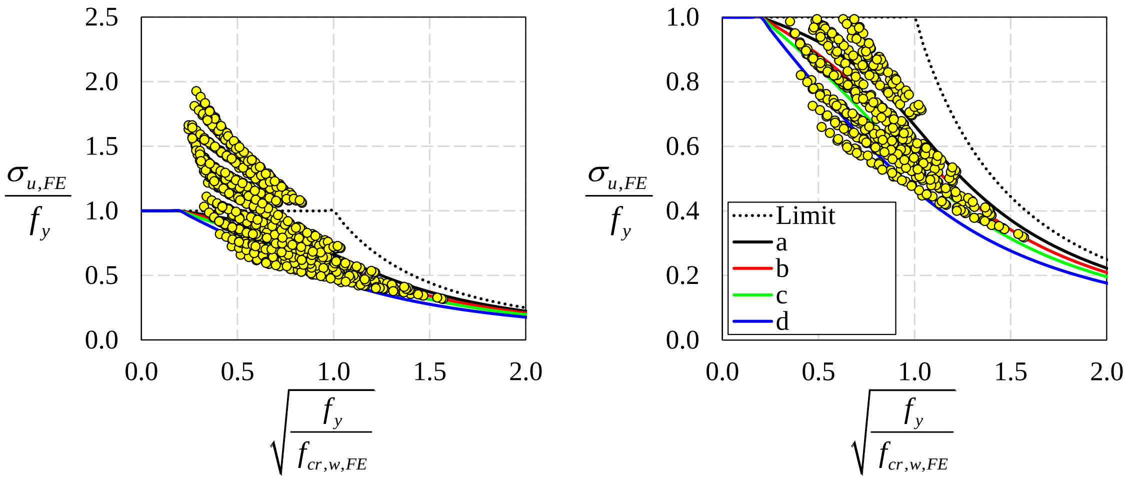

(b) d_0/H=0.70

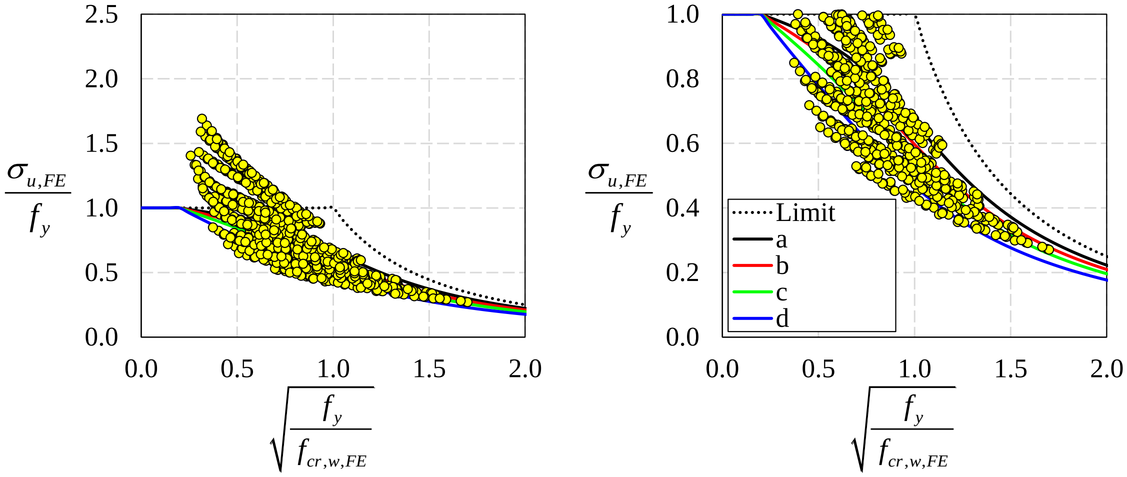

(c) d_o/H=0.75

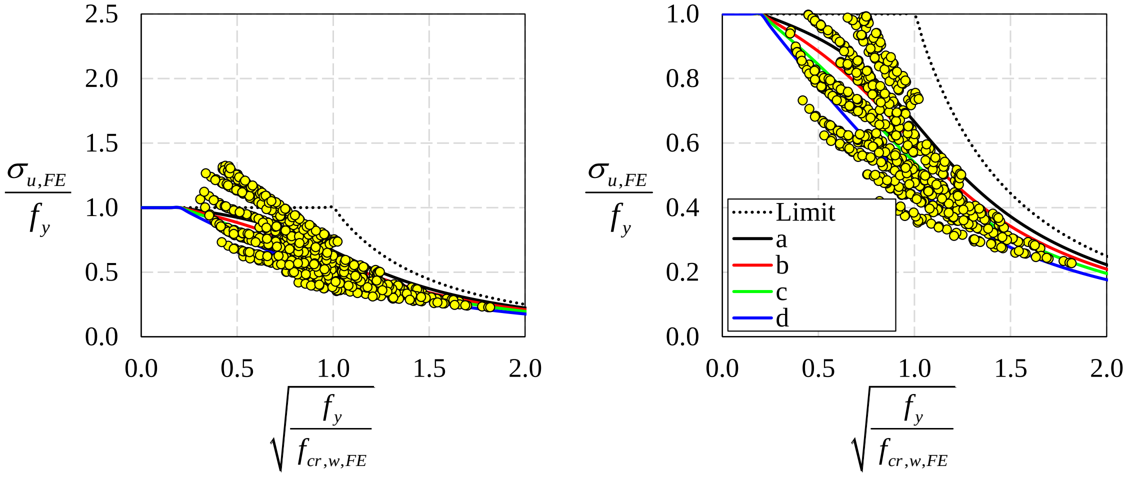

(d) d_o/H=0.80

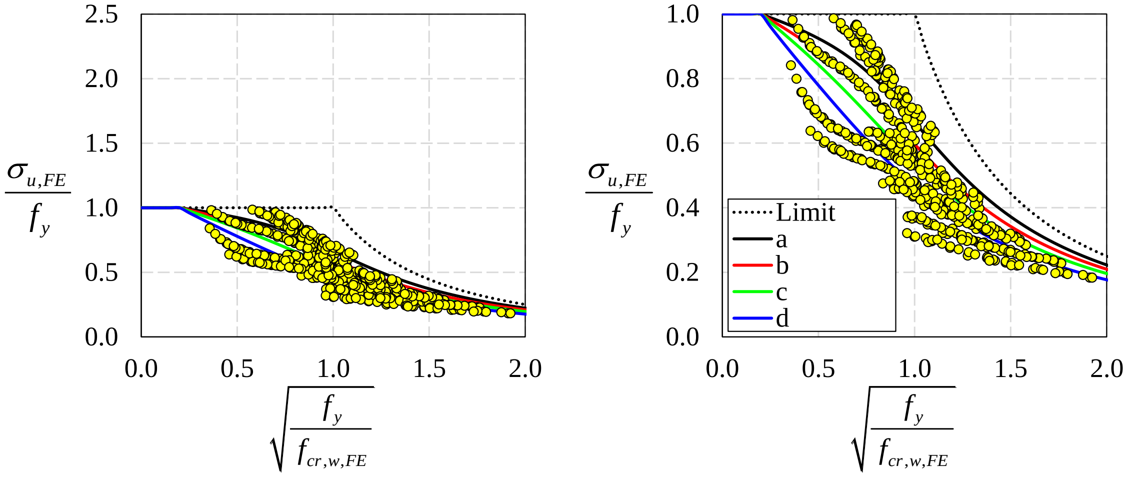

(e) d_o/H=0.85

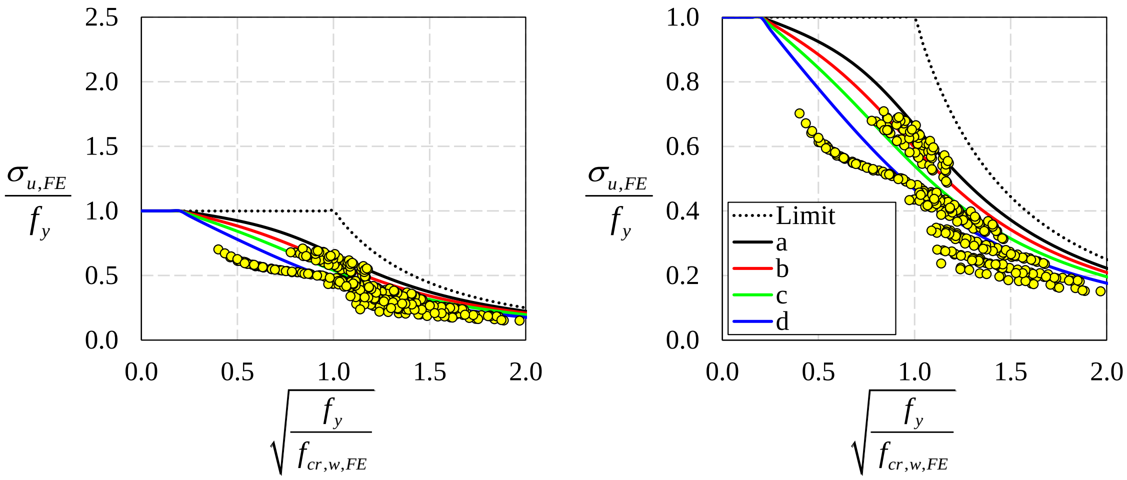

(f) d_o/H=0.90

Fig. 8: d_o/H ratio vs. buckling curves of EC3

3.3 R/d_o ratio

The finite element results normalized with EC3 buckling curves and considered the ratio of the opening radius to opening height are shown in **Fig. 9**. It is important to note that the greater the opening radius, the greater the total height of the opening, as shown in **Fig. 1**. In this context, the results are presented considering R/d_o=0.10 (**Fig. 9a**), R/d_o=0.15 (**Fig. 9b**), R/d_o=0.20 (**Fig. 9c**), R/d_o=0.25 (**Fig. 9d**) and R/d_o=0.30 (**Fig. 9e**).

In this scenario, it is possible to highlight that as the opening radius increases, the resistance further decreases, showing that R/d_o is important in the resistance of steel beams with elliptically-based web openings. For R/d_o=0.10-0.15 and λ_σ<1.0, the maximum values of resistance exceeded the limit value, thus showing that the smaller the radius, the smaller the effective length. On the other hand, the minimum values of capacity resistance were found close to the buckling curve *d*. At last, for R/d_o=0.20-0.30 and $0.5 \leq \lambda_\sigma \leq 2.0$, there was a reduction between the maximum and minimum values of capacity resistance. In this scenario, most of the maximum resistance values were below the buckling curve *a*, and the minimum resistance values were below the buckling curve *d*. These results presented here show that the web-post buckling resistance is sensitive to the parameter R/d_o.

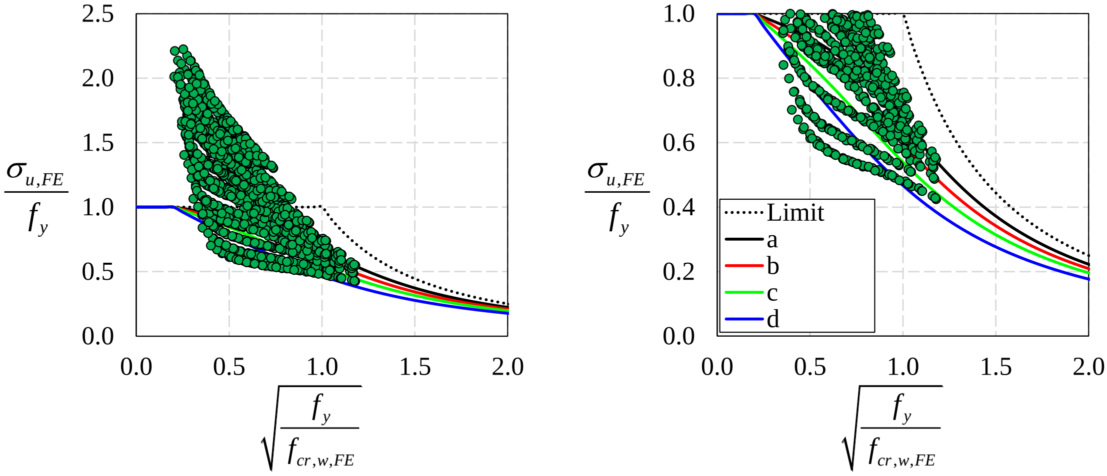

(a) R/d_o=0.10

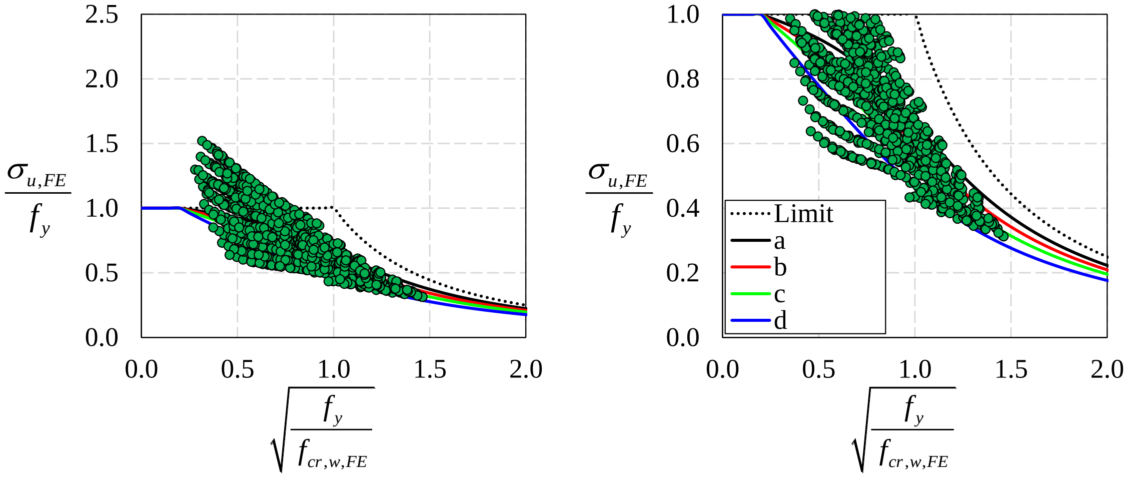

(b) R/d_o=0.15

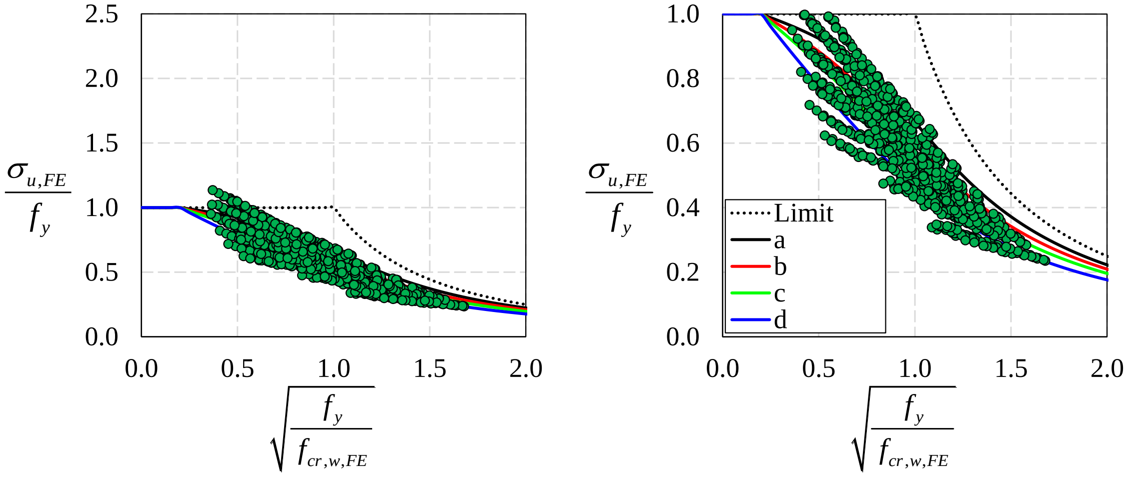

(c) R/d_o=0.20

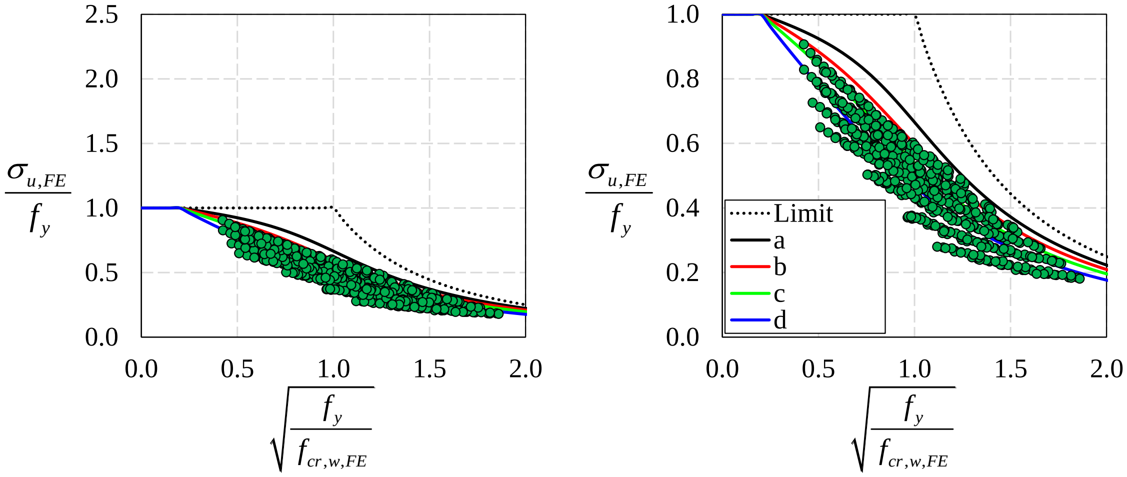

(d) R/d_o=0.25

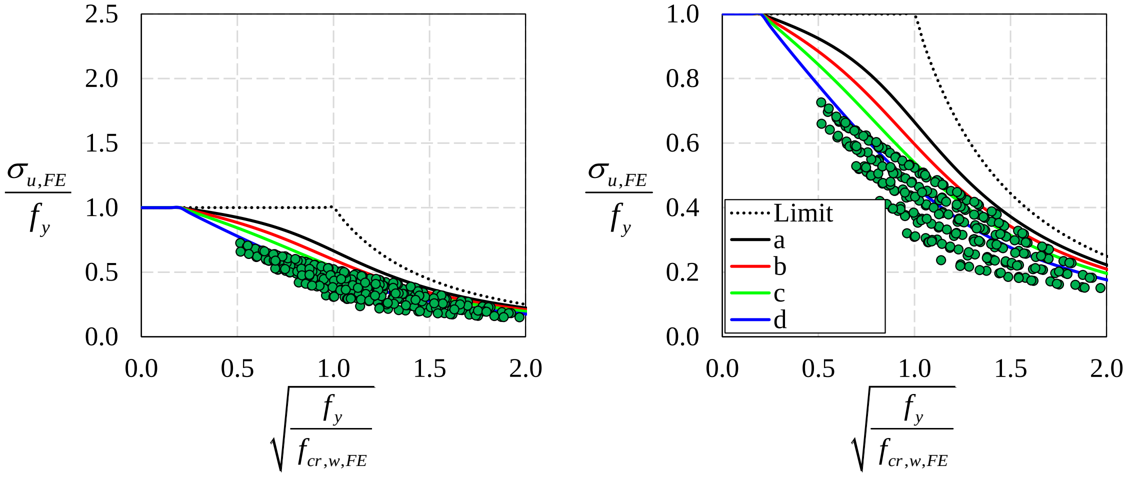

(e) R/d_o=0.30

Fig. 9: R/d_o ratio vs. buckling curves of EC3

3.4 w/d_o ratio

The parameter discussed herein represents the ratio between the width and height of the elliptically-based web opening (**Fig 10**). The ratios studied are w/d_o=0.25 (**Fig. 10a**), w/d_o=0.35 (**Fig. 10b**), w/d_o=0.45 (**Fig. 10c**), w/d_o=0.55 (**Fig. 10d**) and w/d_o=0.65 (**Fig. 10e**). For λ_0<1.0, the maximum resistance values exceeded the limit, while the minimum resistance values remained close to the buckling curve *d*. Another observation that can be highlighted is that is that from w/d_o=0.35, the higher the w/d_o ratio, the greater the resistance. **Fig. 11** illustrates two examples, considering the sections UB 178x102x19 (**Fig. 11a**) and UB 1016x305x487 (**Fig 11b**). Although the H/d, d_o/H and R/d_o

ratios were kept constant for the analysis, the resistance variation as a function of the w/d_o proved to be more sensitive for the UB 1016x305x487, which has a thicker web.

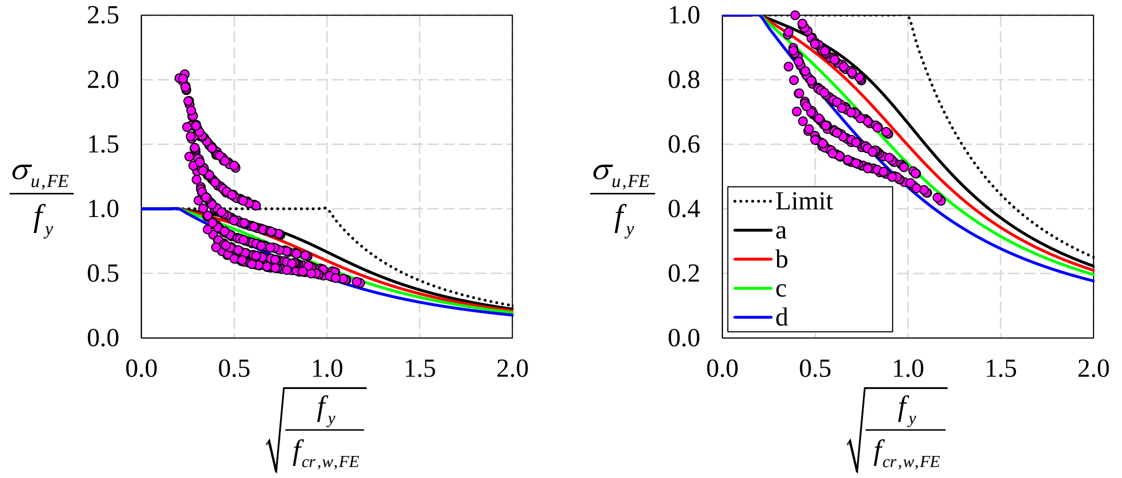

(a) w/d_o=0.25

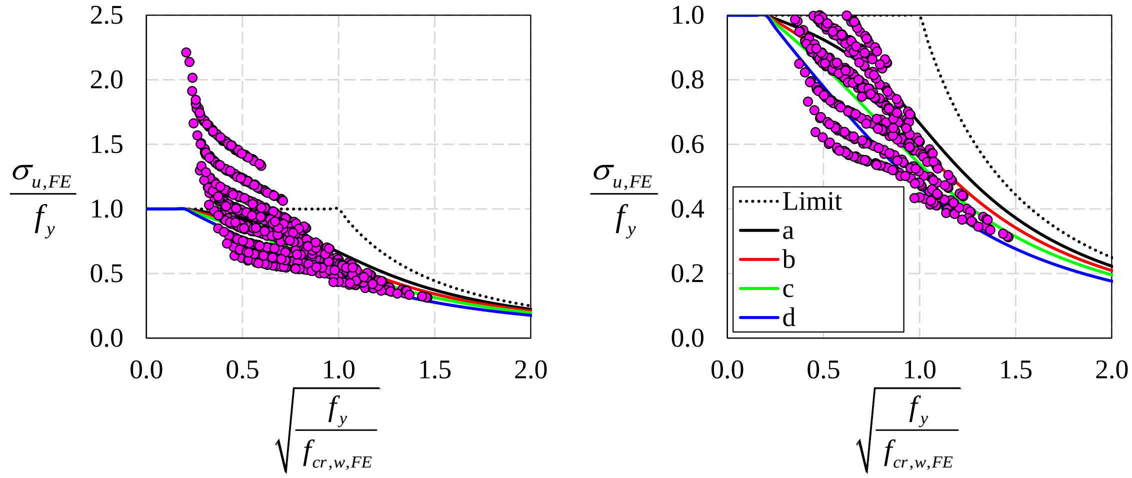

(b) w/d_o=0.35

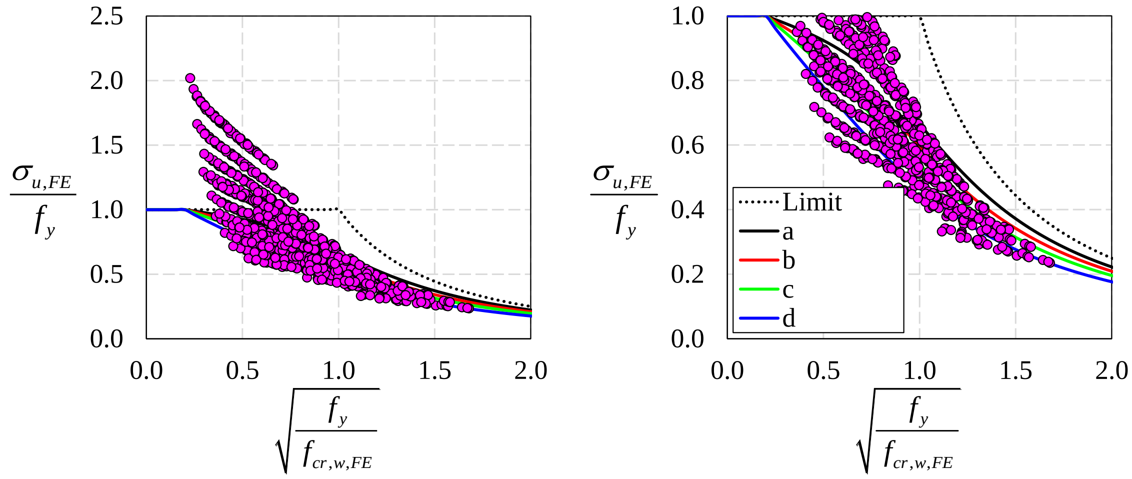

(c) w/d_o=0.45

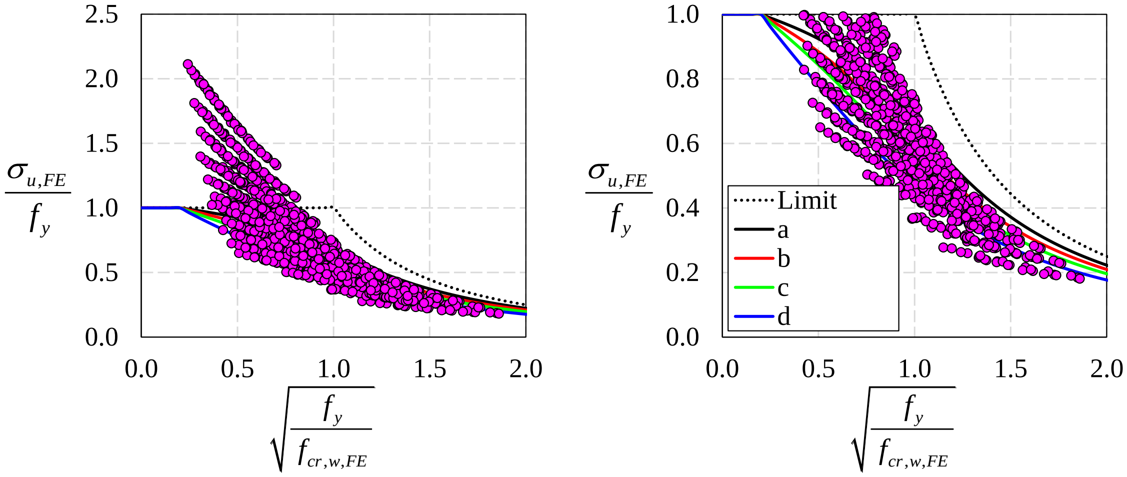

(d) w/d_o=0.55

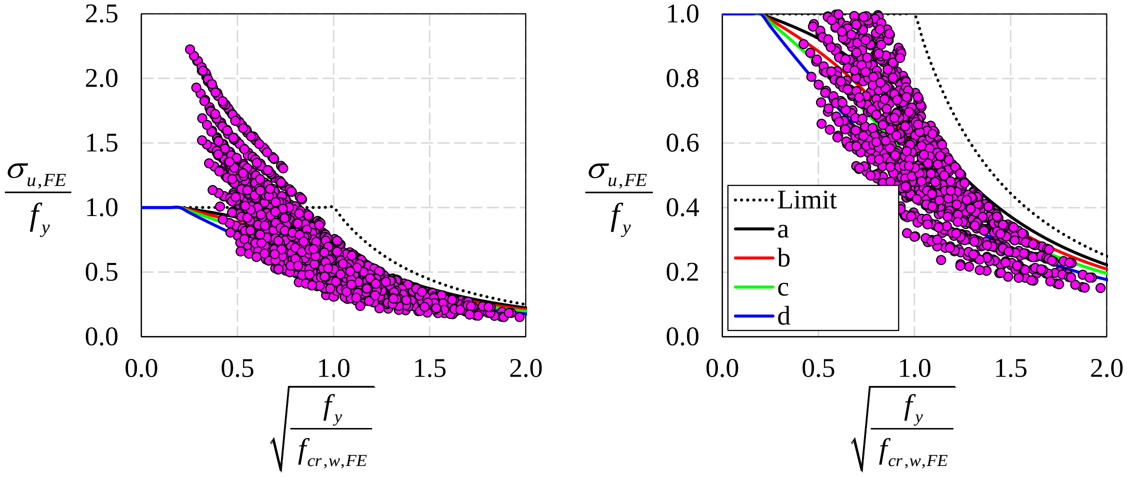

(e) w/d_o=0.65

Fig. 10: *w/d_o* ratio vs. buckling curves of EC3

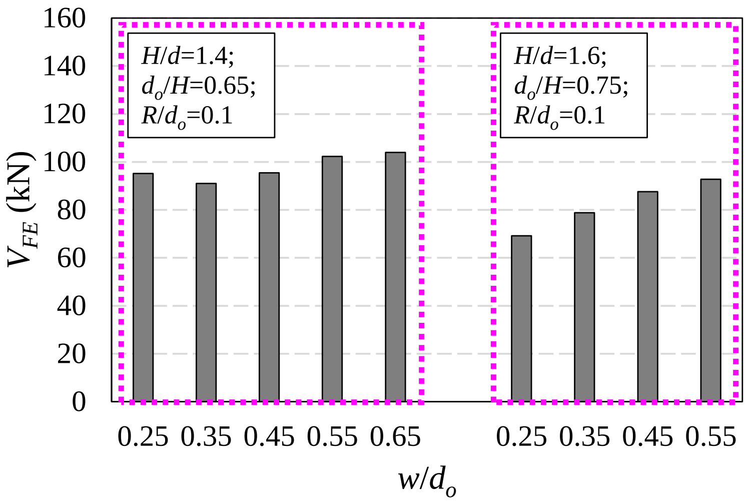

(a) UB 178x102x19

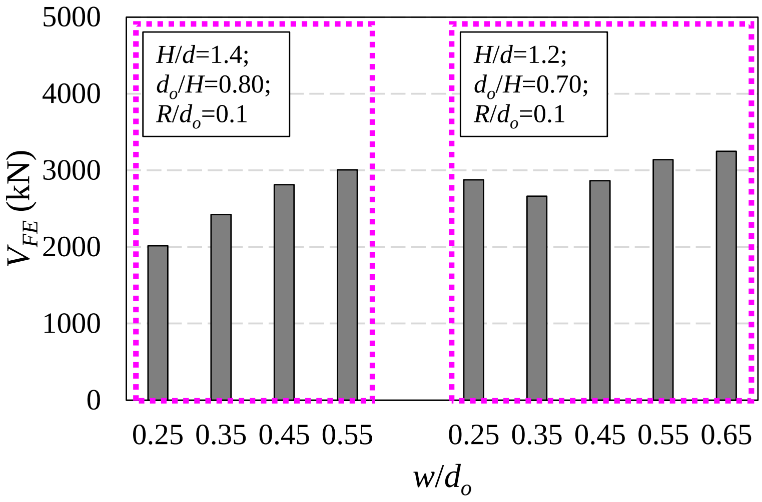

(b) UB 1016x305x487

Fig. 11: Influence of w/d_o on web-post buckling resistance.

4. DESIGN APPROACH

An approach for calculating the web-post buckling resistance of steel beams with elliptically-based web openings is presented. The hypothesis that the buckling occurs within a flexible region, which is delimited by the red dashed lines in the **Fig. 12**. The compressed strut is then defined as seen in the same figure. This is a methodology similar to the one presented in SCI P355 [17], however, effective length of the strut that considers the geometric parameters of the elliptically-based web openings is derived. The numerical effective length from the parametric study is estimated from the critical shear stress acting in the web-post using **Eq. (9)**, then the web-post slenderness is calculated using **Eq. (11)**. Once the web-post slenderness has been determined, the effective length is estimated using **Eq. (12)**.

$$\lambda_{w,FE} = \sqrt{\frac{\pi^2 E}{f_{cr,w,FE}}} = \sqrt{\frac{\pi^2 E}{\frac{V_{cr,FE}}{t_w(s-w)}}} \tag{11}$$

$$l_{eff,FE} = \frac{\lambda_{w,FE} t_w}{\sqrt{12}} \tag{12}$$

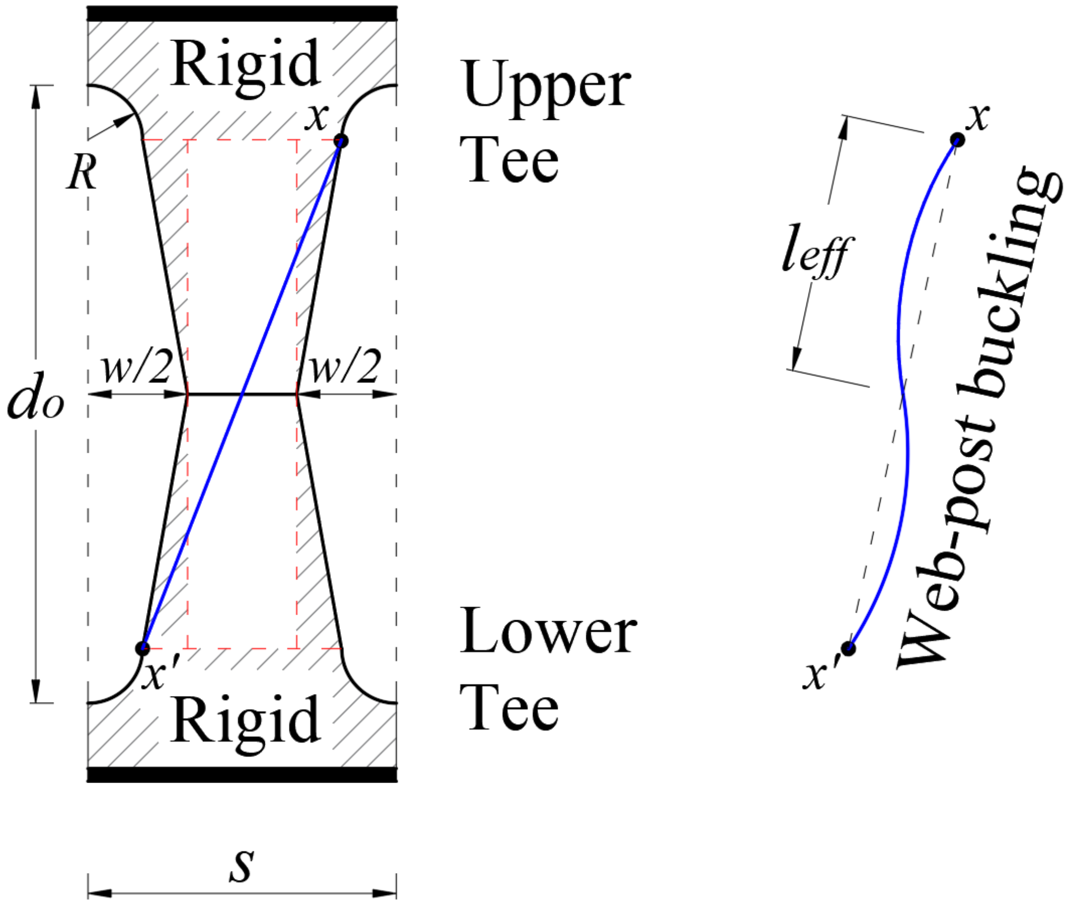

Fig. 12: Approach to effective web-post length (l_{eff})

To define the effective length, a calibration process with the numerical results is required. The effective length would be a function of the cellular beam geometry as well as the tee sections that restrain the buckling of the strut. Once the effective length limit value is determined from the FE results, an approximation of this value is calculated (**Eqs. 13-14**) as a function of the hypothesis presented in **Fig. 12**, in which k is an adjustment factor determined by the linear regression of the studied parameters.

$$l_{eff} = k\sqrt{\left(\frac{d_o - 2R}{2}\right)^2 + \left(\frac{s}{2} - R\right)^2} \tag{13}$$

$$k = 0.516 - 0.288\left(\frac{H}{d_o}\right) + 0.062\left(\frac{s}{s-w}\right) + 2.384\left(\frac{s}{d_o}\right) - 2.906\left(\frac{w}{d_o}\right) \tag{14}$$

In **Fig. 13** the comparison between the values of the effective lengths is presented. **Table 5** shows the statistical analysis of the results for the calculation of the effective length.

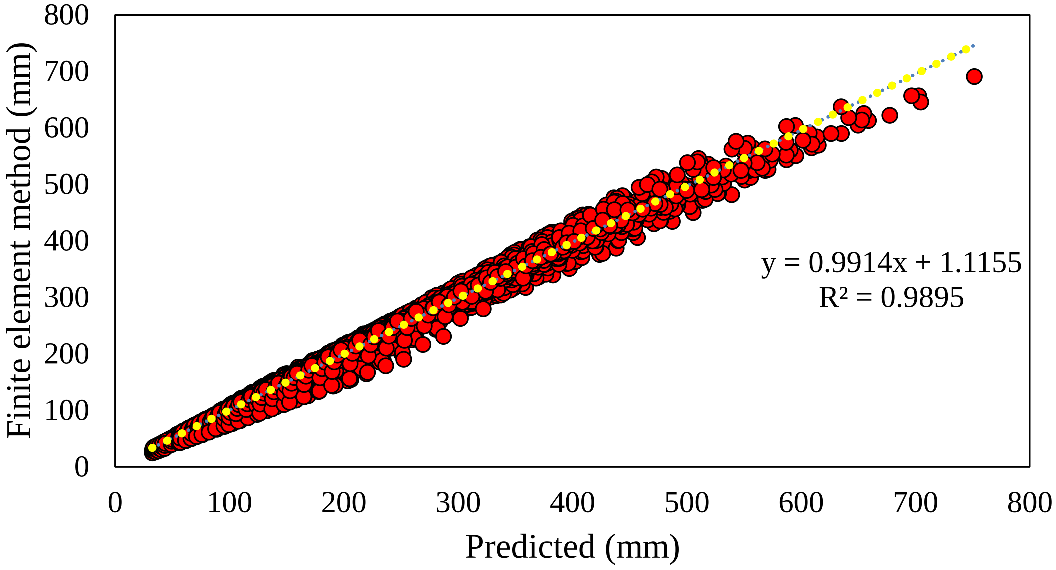

Fig. 13: Effective length – finite element method vs. predicted

Table 5: Statistical analysis for effective length prediction

Analysis	**Value**
R^2 (Regression)	0.9895
RMSE (Root Mean Square Error) (mm)	11.991
MAE (Mean Absolute Error) (mm)	7.954
Minimum relative error	-9.70%
Maximum relative error	34.22%
Average (FEM/Predicted)	0.996
S.D.	5.67%
Var.	0.32%

Once the web-post effective length of perforated steel beams with elliptically-based web openings is determined (**Eqs. 13-14**), the procedure for calculating the web-post buckling resistance, V_{Rk} can be followed, according to **Eqs. (15-22)**, using the buckling curve *c* as shown in **Table 4**:

$$\lambda_w = \frac{l_{eff}\sqrt{12}}{t_w} \tag{15}$$

$$f_{cr,w} = \frac{\pi^2 E}{\lambda_w^2} \tag{16}$$

$$\lambda_0 = \sqrt{\frac{f_y}{f_{cr,w}}} \tag{17}$$

$$\phi = 0.5\left[1 + 0.49(\lambda_0 - 0.2) + \lambda_0^{\,2}\right] \tag{18}$$

$$\chi = \frac{1}{\phi + \sqrt{\phi^2 - \lambda_0^{\,2}}} \le 1.0 \tag{19}$$

$$\sigma_{Rk} = K\chi f_y \tag{20}$$

$$\begin{aligned} K = &-1.318 + 1.790\left(\frac{H}{d_o}\right) + 0.413\left(\frac{s}{s-w}\right) - 1.926\left(\frac{s}{d_o}\right) \\ &+ 0.937\left(\frac{w}{d_o}\right) - 0.02\left(\frac{d_o}{t_w}\right) + 1.412\lambda_0 \end{aligned} \tag{21}$$

$$V_{Rk} = \sigma_{Rk} t_w (s - w) \tag{22}$$

In the next section, the design approach is compared with 4,344 models developed in the parametric study.

5. VERIFICATION

As previously described, in this section the accuracy of the proposed method is verified with the finite element method results. **Fig 14** and **Fig 15** show the normal distribution and the regression analyses, respectively, considering 4,344 models. It is predicted that the mean, standard deviation and variance were 0.982, 7.72% and 0.60%, respectively. The maximum and minimum relative errors between finite element analyses and **Eq. (21)** were -26.89% and 28.02%, respectively. **Table 6** presents the summary of the statistical analysis, also considering the Root Mean Square Error (RMSE) and the Mean Absolute Error (MAE).

It is evident that the proposed novel design equation seems to predict WPB shear capacity of elliptically-based cellular beam results that are in reasonable agreement with the finite element results.

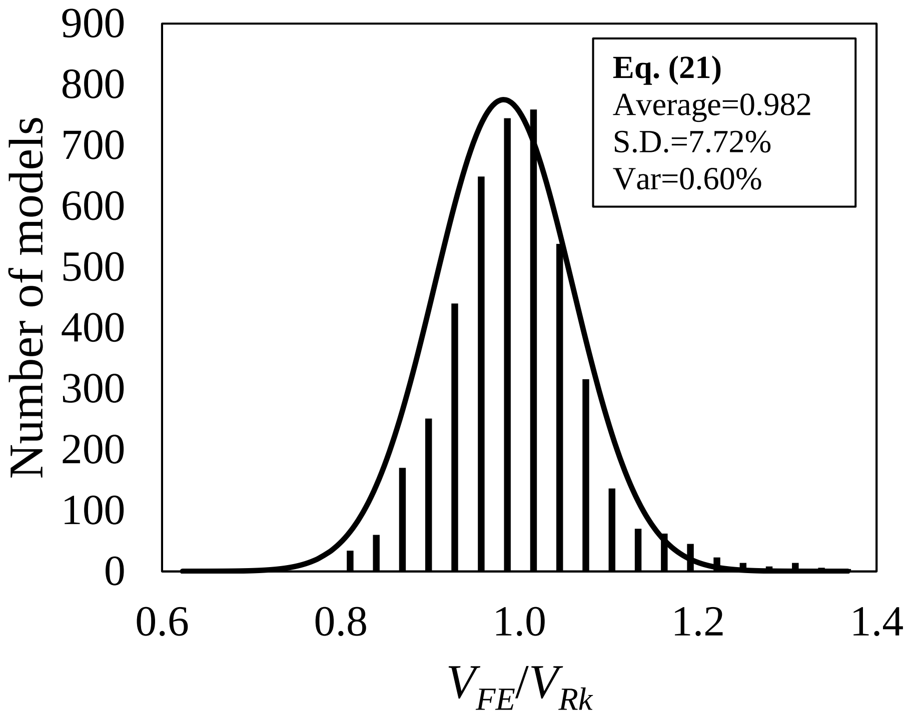

Fig. 14: Normal distribution – Finite element analyses vs. Design Approach

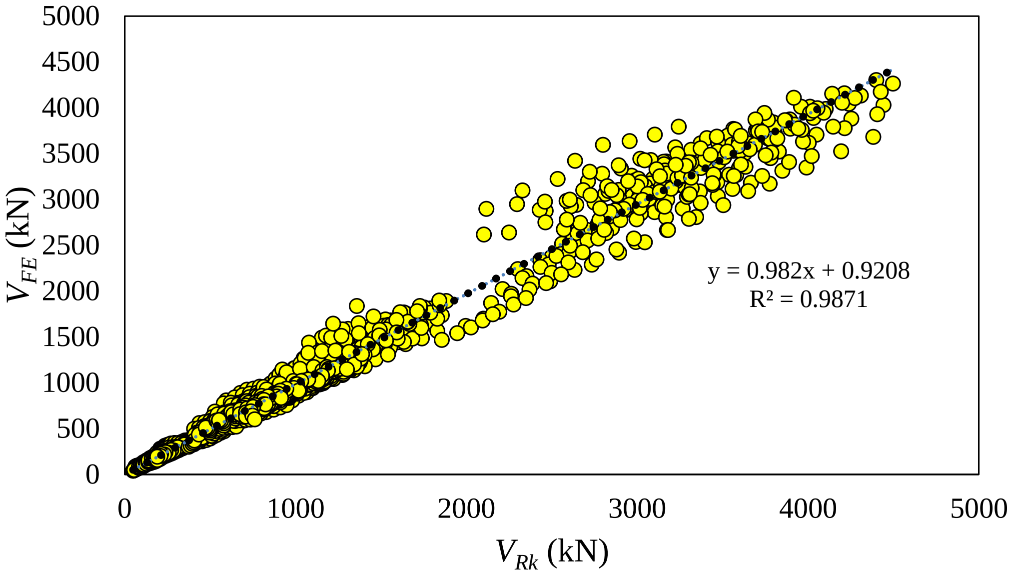

Fig. 15: Web-post buckling resistance – finite element method vs. predicted

Table 6: Statistical analysis for web-post buckling calculation procedure

Analysis	Value
R^2 (Regression)	0.9871
RMSE (Root Mean Square Error) (kN)	91.09
MAE (Mean Absolute Error) (kN)	46.24
Minimum relative error	-26.89%
Maximum relative error	28.02%
Average (FEM/Predicted)	0.982
S.D.	7.71%
Var.	0.59%

6. A STATISTICAL EVALUATION IN THE FASHION OF ANNEX D EN 1990

A statistical analysis following the provisions of Annex D EN 1990 [37] has been carried out in order to assess the reliability of the proposed design method. **Table 7** illustrates the key statistical parameters, including the number of tests and finite element data n, the design fractile factor (ultimate limit state) $k_{d,n}$, the average ratio of FE to model resistance based on a least squares fit to all the data $\bar{b}$, the combined coefficient of variation incorporating both model and basic variable uncertainties Vr and the partial safety factor for cross section resistance γ_{M0}. The material over-strength of high strength steel was taken equal to 1.25 with a coefficient of variation COV of 0.055 [35]. The COV between the experimental and the numerical results, which was found 0.0133, is also considered. The COV for the geometric properties is taken as 0.028. Performing a First Order Reliability Method (FORM) in accordance with the Eurocode target reliability requirements, the partial factor γ_{M0} is 0.96. As the partial factor is close to unity, the value of γ_{M0}=1.00 as recommended in EC3 [18], is appropriate for the design of steel beams with elliptically-based web openings in WPB.

Table 7: Summary of the reliability analysis for the proposed method

n	$\bar{b}$	$k_{d,n}$	V_r	γ_{M0}
4344	0.982	3.04	0.1	0.96

CONCLUDING REMARKS

The present work studies the web-post buckling resistance of perforated steel beams with elliptically-based web openings. A finite element method was developed based on tests from the literature, considering full and single web-post models. A parametric study was carried out using Python to automate data processing. Post-buckling analysis was conducted by geometrically and materially nonlinear analysis with imperfections. From 5,400 geometric models, 4,344 had the failure mode characterized by the WPB. The results were used to propose a design approach for the buckling resistance of the strut model analogy, in which the compressive stress was calculated using EC3 approach. The effective length of elastic buckling was defined and properly calibrated by regression, and the web-post buckling resistance is calculated using the buckling curve c. It was concluded:

i. The smaller the expansion factor (H/d), the smaller the web-post slenderness (λ_w), and consequently, the smaller the effective length (l_{eff}). This causes an increase in capacity resistance.

ii. The lower the height of the elliptically-based web opening (d_o), the greater the capacity resistance. This can be explained in terms of the upper and lower tees sections, that is, the lower the height of the web opening, the greater the height of the tee sections (d_t and d_b), thus increasing the capacity to resist normal and tangential stresses.

iii. As the opening radius (R/d_o) increases, the resistance further decreases, showing that ratio is important in the resistance of steel beams with elliptically-based web openings.

iv. The resistance showed sensitivity as a function of w/d_o ratio. However, this sensitivity can be more significant with the variation of geometric parameters of the section, such as web.

v. The proposed analytical model for the WPB resistance was verified by a reliability analysis and confirmed that it is appropriate for the design of perforated steel beams with elliptically-based web openings.

REFERENCES

[1] ArcelorMittal. ACB® and Angelina® beams - A New Generation of Cellular Beams 2018.

[2] Ferreira FPV, Shamass R, Limbachiya V, Tsavdaridis KD, Martins CH. Lateral–torsional buckling resistance prediction model for steel cellular beams generated by Artificial Neural Networks (ANN). Thin-Walled Struct 2022;170:108592. https://doi.org/10.1016/j.tws.2021.108592.

[3] Ellobody E. Nonlinear analysis of cellular steel beams under combined buckling modes. Thin-Walled Struct 2012;52:66–79. https://doi.org/10.1016/j.tws.2011.12.009.

[4] Panedpojaman P, Sae-Long W, Chub-Uppakarn T. Cellular beam design for resistance to inelastic lateral-torsional buckling. Thin-Walled Struct 2016;99:182–94. https://doi.org/10.1016/j.tws.2015.08.026.

[5] Ellobody E. Interaction of buckling modes in castellated steel beams. J Constr Steel Res 2011;67:814–25. https://doi.org/10.1016/j.jcsr.2010.12.012.

[6] Weidlich CM, Sotelino ED, Cardoso DCT. An application of the direct strength method to the design of castellated beams subject to flexure. Eng Struct 2021;243:112646. https://doi.org/10.1016/j.engstruct.2021.112646.

[7] Ferreira FPV, Martins CH. LRFD for Lateral-Torsional Buckling Resistance of Cellular Beams. Int J Civ Eng 2020;18:303–23. https://doi.org/10.1007/s40999-019-00474-7.

[8] Morkhade SG, Gupta LM. Experimental investigation for failure analysis of steel beams with web openings. Steel Compos Struct 2017;23:647–56. https://doi.org/10.12989/SCS.2017.23.6.647.

[9] Kerdal D, Nethercot DA. Failure modes for castellated beams. J Constr Steel Res 1984;4:295–315. https://doi.org/10.1016/0143-974X(84)90004-X.

[10] Grilo LF, Fakury RH, Castro e Silva ALR de, Veríssimo G de S. Design procedure for the web-post buckling of steel cellular beams. J Constr Steel Res 2018;148:525–41. https://doi.org/10.1016/j.jcsr.2018.06.020.

[11] Tsavdaridis KD, D'Mello C. Web buckling study of the behaviour and strength of perforated steel beams with different novel web opening shapes. J Constr Steel Res 2011;67:1605–20. https://doi.org/10.1016/j.jcsr.2011.04.004.

[12] Limbachiya V, Shamass R. Application of Artificial Neural Networks for web-post shear resistance of cellular steel beams. Thin-Walled Struct 2021;161:107414. https://doi.org/10.1016/j.tws.2020.107414.

[13] Panedpojaman P, Thepchatri T, Limkatanyu S. Novel design equations for shear strength of local web-post buckling in cellular beams. Thin-Walled Struct 2014;76:92–104. https://doi.org/10.1016/j.tws.2013.11.007.

[14] Fares SS, Coulson J, Dinehart DW. AISC Steel Design Guide 31: Castellated and Cellular Beam Design. American Institute of Steel Construction; 2016.

[15] American Institute of Steel Construction. ANSI/AISC 360-16 - Specification for structural steel buildings. 2016.

[16] Ward JK. Design of Composite and Non-Composite Cellular Beams. Silwood Park, Ascot, UK: Steel Construction Institute; 1990.

[17] Lawson RM, Hicks SJ. Design of composite beams with large web openings. SCI P355. The Steel Construction Institute; 2011.

[18] European committee for standardization. EN 1993-1-1: Eurocode 3 – Design of steel structures – Part 1-1: General rules and rules for buildings 2002.

[19] Tsavdaridis KD, D'Mello C. FE Investigation of Perforated Sections with Standard and Non-Standard Web Opening Configurations and Sizes. In: Chan SL, editor. 6th Int. Conf. Adv. is Steel Struct., Hong Kong, China: Hong Kong Institute of Steel Construction; 2009, p. 213–20.

[20] Tsavdaridis KD. Structural performance of perforated steel beams with novel web openings and with partial concrete encasement. City University London; 2010.

[21] Tsavdaridis KD, Kingman JJ, Toropov V V. Application of structural topology optimisation to perforated steel beams. Comput Struct 2015;158:108–23. https://doi.org/10.1016/j.compstruc.2015.05.004.

[22] Tsavdaridis KD, D'Mello C. Vierendeel Bending Study of Perforated Steel Beams with Various Novel Web Opening Shapes through Nonlinear Finite-Element Analyses. J Struct Eng 2012;138:1214–30. https://doi.org/10.1061/(asce)st.1943-541x.0000562.

[23] Tsavdaridis KD, D'Mello C. Optimisation of novel elliptically-based web opening shapes of perforated steel beams. J Constr Steel Res 2012;76:39–53. https://doi.org/10.1016/j.jcsr.2012.03.026.

[24] Tsavdaridis KD, D'Mello C. Structural beam. GB 2492176, 2012.

[25] Zaarour W, Redwood R. Web Buckling in Thin Webbed Castellated Beams. J Struct Eng 1996;122:860–6. https://doi.org/10.1061/(ASCE)0733-9445(1996)122:8(860).

[26] Tsavdaridis KD, Galiatsatos G. Assessment of cellular beams with transverse stiffeners and closely spaced web openings. Thin-Walled Struct 2015;94:636–50. https://doi.org/10.1016/j.tws.2015.05.005.

[27] Durif S, Bouchaïr A, Vassart O. Experimental and numerical investigation on web-post specimen from cellular beams with sinusoidal openings. Eng Struct 2014;59:587–98. https://doi.org/10.1016/j.engstruct.2013.11.021.

[28] Ferreira FPV, Tsavdaridis KD, Martins CH, De Nardin S. Buckling and post-buckling analyses of composite cellular beams. Compos Struct 2021;262. https://doi.org/10.1016/j.compstruct.2021.113616.

[29] Ferreira FPV, Martins CH, De Nardin S. Sensitivity Analysis of Composite Cellular Beams to Constitutive Material Models and Concrete Fracture. Int J Struct Stab Dyn 2021;21:2150008. https://doi.org/10.1142/S0219455421500085.

[30] Ferreira FPV, Tsavdaridis KD, Martins CH, De Nardin S. Ultimate strength prediction of steel–concrete composite cellular beams with PCHCS. Eng Struct 2021;236:112082. https://doi.org/10.1016/j.engstruct.2021.112082.

[31] Ferreira FPV, Rossi A, Martins CH. Lateral-torsional buckling of cellular beams according to the possible updating of EC3. J Constr Steel Res 2019;153:222–42. https://doi.org/10.1016/j.jcsr.2018.10.011.

[32] Ferreira FPV, Martins CH, De Nardin S. Assessment of web post buckling resistance in steel-concrete composite cellular beams. Thin-Walled Struct 2021;158:106969. https://doi.org/10.1016/j.tws.2020.106969.

[33] Ferreira FPV, Tsavdaridis KD, Martins CH, De Nardin S. Composite action on web-post buckling shear resistance of composite cellular beams with PCHCS and PCHCSCT. Eng Struct 2021;246:113065. https://doi.org/10.1016/j.engstruct.2021.113065.

[34] Rajana K, Tsavdaridis KD, Koltsakis E. Elastic and inelastic buckling of steel cellular beams under strong-axis bending. Thin-Walled Struct 2020;156:106955. https://doi.org/10.1016/j.tws.2020.106955.

[35] Shamass R, Guarracino F. Numerical and analytical analyses of high-strength steel cellular beams: A discerning approach. J Constr Steel Res 2020;166:105911. https://doi.org/10.1016/j.jcsr.2019.105911.

[36] Yun X, Gardner L. Stress-strain curves for hot-rolled steels. J Constr Steel Res 2017;133:36–46. https://doi.org/10.1016/j.jcsr.2017.01.024.

[37] European committee for standardization. EN 1990: Eurocode – Basis of structural design n.d.